HHS Public Access

Author manuscript

Sci Immunol. Author manuscript; available in PMC 2026 March 19.

Published in final edited form as:

Sci Immunol. 2025 November 07; 10(113): eadm7800. doi:10.1126/sciimmunol.adm7800.

Th17 cells converted into ex-Th17 cells sustain rheumatoid-like IL-17-independent inflammatory arthritis

Martina Zoccheddu[1], **Kensuke Suga**[2,*], **Amara Seng**[2,*], **Mattias N. D. Svensson**[1,3], **Paramita Dutta**[4], **Sanaz Panahandeh**[5], **Hadijat-Kubura Moradeke Makinde**[6], **Myungja Ro**[1,2], **Yizhou Wang**[5], **Hyobin Kim**[5], **Zbigniew Mikulski**[7], **Katarzyna Dobaczewska**[7], **Francesca Ingegnoli**[8], **Ruth Minsha**[6], **John F Seagrist**[6], **Mary Carns**[6], **Kathleen Aren**[6], **Salina Dominguez**[6], **Mohammad Daud Khan**[6], **Angela Denn**[7], **Roberto Caporali**[8], **Pietro Simone Randelli**[9], **David A McBride**[10], **Arthur M Mandelin II**[6], **Carla Marie Cuda**[6], **Zhiping Paul Wang**[5], **Jason H. Moore**[5], **Nisarg J. Shah**[10], **Kyoung Jae Won**[5], **Deborah Winter**[6], **Ferhat Ay**[4,11], **Harris Perlman**[6], **Nunzio Bottini**[1,2]

[1]Department of Medicine, Division of Rheumatology, Allergy and Immunology, University of California, San Diego; La Jolla, CA 92093, USA

[2]Dept. of Medicine, Kao Autoimmunity Institute and Division of Rheumatology, Cedars-Sinai Medical Center, Los Angeles, CA 90048, USA

[3]Department of Rheumatology and Inflammation Research, Sahlgrenska Academy, Institute of Medicine, University of Gothenburg, Gothenburg 41346, Sweden

[4]Centers for Autoimmunity, Inflammation and Cancer Immunotherapy, La Jolla Institute for Immunology, 9420 Athena Circle, La Jolla, CA, 92037, USA

[5]Department of Computational Biomedicine, Cedars-Sinai Medical Center, Los Angeles, CA 90048, USA

[6]Department of Medicine, Division of Rheumatology Northwestern University Feinberg School of Medicine, Chicago, IL 60611, USA

[7]Histology and Microscopy Core Facility, La Jolla Institute for Immunology, La Jolla, CA 92037, USA

[8]Clinical Rheumatology Unit, ASST Gaetano Pini-CTO, Dept. of Clinical Sciences & Community Health, Università degli Studi di Milano, Milan, Italy

[9]1st Orthopedic Unit, ASST Gaetano Pini-CTO, Lab of Applied Biomechanics, Department of Biomedical Sciences for Health, Università degli Studi di Milano, Milan, Italy

Correspondence to be addressed to Nunzio Bottini, MD, PhD, nunzio.bottini@cshs.org.

*Equal contribution

Author contributions: Conceptualization: N. Bottini and F. Ay. Formal analysis: P. Dutta, S. Panahandeh, M. Ro, Y. Wang, H. Kim, S. Dominguez, M. D. Khan, N. Shah, C. M. Cuda, D. Winter. and F. Ay. Funding acquisition: N. Bottini. Investigation: M. Zoccheddu, K. Suga, A. Seng, M. N. D. Svensson, H-K. M. Makinde, M. Ro, Z. Mikulski, K. Dobaczewska, A. Denn, D. A. McBride and N. Shah. Methodology: K. Suga and M. N. D. Svensson. Project administration: R. Minsha, J.F. Seagrist, M. Carns, K. Aren and N. Bottini. Resources: F. Ingegnoli, R. Caporali, P.D. Randelli and A. Mandelin, Software: K.J. Won, and F. Ay. Supervision: Z.P. Wang, J.H. Moore, K.J. Won, F. Ay, H. Perlman and N. Bottini. Validation: M. Ro. Visualization: M. Zoccheddu, K. Suga, A. Seng, M. Ro, P. Dutta and S. Panahandeh. Writing—original draft: by M. Zoccheddu, F. Ay and N. Bottini. Writing—review and editing: by M. Zoccheddu, K. Suga, A. Seng, and N. Bottini. All authors have reviewed and approved the final version of the manuscript.

Competing interests: Authors declare that they have no competing interests.

[10]Department of Nanoengineering, University of California, San Diego, La Jolla, CA 92093, USA

[11]Department of Pediatrics, University of California San Diego, La Jolla, CA, 92093, USA

Abstract

T helper 17 (Th17) cells are found in the periphery and synovium of rheumatoid arthritis (RA) patients, however IL-17-targeted interventions have limited efficacy in established RA. Inflammation can induce Th17 cell transdifferentiation into IL-17-negative exTh17 cells but the role of exTh17 cells in arthritis is unknown. We performed Th17 cell lineage tracing in the SKG mouse model of RA. In arthritic mice, synovial Th17 cells transdifferentiate into $CD44^+$ exTh17 cells, which are more arthritogenic and sustain inflammation that is IL-17-independent. The exTh17 cell gene signature includes upregulation of CD44 and S1PR4 and correlates with the profile of human RA synovial $CD4^+$ T cells. We demonstrate that crosstalk between Th17 cells and fibroblast-like synoviocytes (FLS) via S1P promotes Th17-exTh17 cell conversion. CD44 is necessary for exTh17 cell-mediated arthritis. Our study suggests that FLS expansion during RA progression promotes Th17-exTh17 cell conversion. These results could potentially enable RA precision therapy.

One-sentence summary

exTh17 cells drive IL-17-independent chronic SKG arthritis in mice through upregulation of CD44 and S1PR4 and crosstalk with FLS.

INTRODUCTION

$CD4^+$ T cells expressing interleukin (IL)-17 family cytokines (Th17 cells) are critical to the maintenance of gut homeostasis and play a role in different inflammatory and autoimmune disorders(1). Since their discovery and the identification of RORγt as their master transcription factor(2–4), several studies have shown that Th17 cells display considerable complexity and are exquisitely sensitive and adaptable to their microenvironment. Recent single-cell genomic studies have elucidated the heterogeneity of Th17 cells as a key a feature of both protective (tissue homeostatic) as well as pathogenic Th17 cells, which is reflected in immunometabolic differences between these populations(5). In response to microenvironmental cues, Th17 cells can undergo immunophenotypic changes. Fate-mapping studies in mice have demonstrated that Th17 cells can differentiate into Th1-like cells characterized by expression of IFNγ or express IL-10 or FoxP3, which leads to the acquisition of a regulatory T cell (Treg)-like phenotype(1). Human Th17 cells are also known to display plasticity and switch to an $IFN\gamma^+$ phenotype after IL-12 stimulation(6).

In rheumatoid arthritis (RA), the role of IL-17 and Th17 cells has not been completely clarified. Early studies identified IL-17 in RA synovium and IL-17 and Th17 cells in RA synovial fluid(7–9). IL-17 also plays a role in the initiation or progression of disease in several mouse models of RA (reviewed in(10)) and Th17 cells are pathogenic in the K/BxN, collagen-induced arthritis (CIA) and the SKG models(10, 11). However, sekukinumab and ixekizumab have shown limited efficacy in RA patients with inadequate responses to disease modifying anti-rheumatic agents (DMARD) methotrexate(12) or TNF inhibitors(13,

14). Recent single-cell genomics surveys of RA synovium, such as the one within the Accelerating Medicines Partnership (AMP) initiative(15), have demonstrated a very low frequency of IL-17-expressing cells in the synovium of patients with established RA. One explanation proposed for these unexpected results is that IL-17 plays a role in the initiation of RA inflammation but becomes less relevant in established RA as the rheumatoid inflammatory milieu tends to convert Th17 cells into IL-17-negative exTh17 cells. IFNγ^{+}RORC^{+}IL-17^{low} "human exTh17 cells" (characterized by expression of CD161, CCR6, and CXCR3) are found in the synovial fluid of juvenile arthritis and RA patients(16, 17). Human exTh17 cells were shown to produce higher levels of TNF and predict response to tumor necrosis factor α (TNF) inhibition in RA(17). A single Th17 cell fate-mapping study has been carried out by Hirota et al. and showed the presence of IL-17^{-}IFNγ^{-} exTh17 cells in the synovium of C.SKG.IL17cre.R26ReYFP mice with early arthritis(18). However, the phenotype of synovial exTh17 cells and whether these cells are pathogenic was not determined.

SKG mice have emerged as a leading model to study the potential role of CD4 T cells in RA. These mice carry a homozygous loss of function W163C mutation in the proximal SH2 domain of ZAP70, initially observed in a BALB/c colony in the Sakaguchi laboratory(19). The ZAP70 mutation impairs negative selection through altered thymic TCR signaling leading to the emergence of autoreactive T cells that differentiate into IL-17^{+}CCR6^{+}TCRα/β^{+} (Th17 cells) and drive spontaneous synovial inflammation starting around 8 weeks of age(19, 20). Arthritis can be transferred to immunodeficient (SCID or Rag2$^{-/-}$ mice) mice by SKG CD4 thymocytes or peripheral T cells(19, 21, 22). The development of arthritis can be accelerated and synchronized through a single intraperitoneal (i.p.) injection of the fungal wall components zymosan or mannan(23, 24). SKG arthritis requires a homozygous Zap70^{SKG} genotype and the H2^{d} haplotype; C57BL/6 (B6) SKG/SKG mice have some markers of autoimmunity but do not develop arthritis(25). Several clinical and pathological aspects of SKG arthritis closely resemble human RA. SKG mice develop chronic symmetric arthritis with prominent involvement of small and medium paw joints, which is erosive (19). They also display rheumatoid factor (RF)(19) and anti-citrullinated peptide Ab(26). Arthritic SKG synovium displays an abundant infiltrate of CD4 T cells and prominence of fibroblast-like synoviocytes (FLS)(18). FLS are joint-lining stromal cells that are dramatically expanded in RA synovium and are known to promote arthritis by amplifying immune mediated inflammation and mediating cartilage and bone damage(27). Female mice develop more severe disease than male mice, reflecting the sex bias found in human RA(19). Knockout (KO) of IL-1, TNF or IL-6, three cytokines that are recognized drug targets for RA, all impair development of arthritis in SKG mice(28).

KO of IL-17 eliminates arthritis in SKG mice and expression of IL-17 is necessary for induction of arthritis in Rag2$^{-/-}$ mice after adoptive transfer of SKG CD4 T cells(29), pointing to IL-17 and Th17 cells as critical for initiation of arthritis in this model. It is not yet clear if IL-17 is necessary for maintenance of chronic arthritis, which reflects the typical condition of RA patients after failure of DMARDs. We have revisited Th17 cell fate mapping in SKG mice and have focused on the phenotype and pathogenic role of exTh17 cells. In a previous study examining FoxP3^{+} Treg stability, we have shown that congenic B6.ZAP70$^{Skg/Skg}$ mice develop arthritis at a severity comparable to SKG mice on a BALB/c

background once made congenic for homozygous $H2^d$ haplotype to yield B6.ZAP70$^{Skg/Skg}$.H2$^{d/d}$ (called B6.SGK.H2d) mice(30). Here, we have leveraged B6.SKG.H2d mice to apply a lineage-tracing approach to the conversion of Th17 cells into exTh17 cells in arthritic SKG mice. We show that in chronic SKG arthritis, synovial Th17 cells are replaced by a population of IFNγ^-IL-10$^-$ exTh17 cells, which becomes the most prominent CD4 T cell subset and can be transferred to cause arthritis symptoms more efficiently than Th17 cells . The application of cutting-edge genomic techniques, including multiome sequencing and spatial transcriptomics, allowed us to demonstrate that SKG exTh17 cells display transcriptional signatures that have correlates with human RA synovial T cells. We also find that FLS can drive conversion of Th17 cells into exTh17 cells and identify pathways regulating the conversion of Th17 cells into exTh17 cells and the pathogenic effect of exTh17 cells in arthritis.

RESULTS

Th17 cells convert into exTh17 cells and become the most prominent T cell population in joints and lymph nodes of SKG mice with chronic arthritis.

To explore the development and role of exTh17 cells in inflammatory arthritis, we bred B6.SKG.H2d mice(30) with the IL17cre driver generated by the Stockinger group(31), with Vert-X (carrying a IL-10-eGFP reporter)(32), GREAT (carrying a IFNγ-YFP reporter(33)), and Ai14 mice (carrying an inducible tdTomato cassette in the ROSA26 locus(34)). CD4 T cells from the resulting Il17$^{Cre/+}$Ifng$^{YFP/YFP}$Il10$^{eGFP/eGFP}$R26R$^{tdTom/TdTom}$ZAP70$^{SKG/SKG}$.H2$^{d/d}$ (h triTh17) mice were transferred into B6.Rag2$^{-/-}$.H2$^{d/d}$ (see ref.(30), Rag2-KO) mice. At 7 days after CD4 T cell transfer, mice were stimulated with mannan to accelerate arthritis development (Fig. 1A,B and fig. S1A, B). Rag2-KO mice recipients of triTh17 CD4 T cells (Rag2-KO-CD4) developed arthritis with clinical and histopathologic features, including synovitis, cartilage depletion and bone erosion, similar to that observed in spontaneous SKG arthritis (Fig. 1C-F and fig. S1C-F)(30). No differences in severity of arthritis were seen between male and female Rag2-KO-CD4 mice (fig. S1G). To dynamically map the fate of Th17 cells in this model we assessed the frequency of CD4 T cells that were Th17 cells (IL17$^+$tdTomato$^+$), exTh17-IFNγ^+ (IL17$^-$tdTomato$^+$YFP$^+$), exTh17-IL-10$^+$ (IL17$^-$tdTomato$^+$eGFP$^+$), as well as, Th1-like IFNγ^+ (IL17$^-$tdTomato$^-$YFP$^+$) and Tr1-like (IL17$^-$tdTomato$^-$eGFP$^+$) cells in the joints and lymph nodes of recipient mice. Mice were assessed at day 7 (pre-arthritic), day 21 (early arthritis), day 42 (arthritis plateau) and day 69 (chronic arthritis) after the adoptive transfer (Fig. 1G, H, and fig. S2). The frequency of Th17 cells in arthritic joints and joint-draining lymph nodes peaked at day 42. Th1-like IL17$^-$ IFNγ^+ cells were the most prominent population in pre-arthritic (before mannan induction) joints and draining lymph nodes but their frequency rapidly decreased during the course of arthritis to become almost undetectable in the chronic phase. Tr1-like IL17$^-$ IL-10$^+$ cells were less represented but showed a trend similar to Th1-like cells. exTh17 cells constituted 20% and 10% of the T cells respectively in arthritic ankle joints and draining lymph nodes in the pre-arthritic phase, and their frequency increased in parallel to clinical severity to represent most T cells in joints and lymph nodes in the chronic phase. Within the exTh17 cell population, very few cells with an exTh17-IL-10$^+$ phenotype could be found in joints or lymph nodes at any

time. exTh17-IFNγ^+ cells represented the majority of exTh17 cells in the pre-arthritic phase, but rapidly disappeared in the chronic phase. Gene expression studies of sorted Th17 and exTh17 cells from chronically arthritic mice confirmed lack of *Il17a* expression in exTh17 cells, however there were no differences in *Rorc* expression between Th17 and exTh17 cells. Of note, exTh17 cells showed a distinct upregulation of *Il6* and *Tfna*, known pathogenic cytokines in SKG arthritis and human RA (Fig.1l)(28, 35, 36). We conclude that in the SKG model of inflammatory arthritis, Th17 cells can lose expression of IL-17a and may convert into exTh17 cells, which become a prominent T cell population in chronic arthritis. Our study also suggests that the majority of exTh17 cells in arthritic joints and lymph nodes of arthritic mice lack expression of IFNγ or IL-10, in contrast to exTh17 cells populations described in the nervous system or intestinal inflammation(37).

ExTh17 cells display higher arthritogenic potential than Th17 cells which does not depend on re-expression of IL-17.

To compare the arthritogenic potential of Th17 and exTh17 cells, we sorted Th17 and exTh17 cells from arthritic Rag2-KO-CD4 at day 63 to 69 after the transfer and performed a secondary adoptive transfer of 1×10^5 Th17 or exTh17 cells into Rag2-KO (the recipient are Rag2-KO-Th17 and Rag2-KO-exTh17, respectively) followed by arthritis acceleration via mannan injection at day 7 after cell transfer (Fig. 2a). Both Rag2-KO-Th17 and Rag2-KO-exTh17 developed substantial arthritis. However, the clinical and histopathologic severity of arthritis was higher in Rag2-KO-exTh17 mice (Fig. 2B-D and fig. S3A). Consistent with these data, there were higher inflammatory cell counts Rag2-KO-exTh17 mice (fig. S3B) Gene expression on whole joint homogenates from Rag2-KO-Th17 vs Rag2-KO-exTh17 with chronic arthritis showed similar expression *Rorc (*Fig. 1I)Rag2-KO-exTh17 had increased expression of *Il6* and *Tnfa*, as well as RA-relevant matrix metalloproteases, *Mmp2* and *Mmp3*(27) and *Cxcl13,* a chemokine associated with formation of ectopic lymphoid nodes in the synovium of RA patients and SKG mice(30, 38)(Fig. 2E). Immunophenotyping of the joint draining lymph nodes showed exTh17 cells made up the vast majority of CD4 T cells in both Rag2-KO-Th17 and Rag2-KO-exTh17 mice (Fig. 2F). Similar data was obtained in male and female recipient mice (fig. S3C, D). These data point to a higher arthritogenic potential of exTh17 cells compared to Th17 cells in SKG arthritis and suggest that exTh17 cell pathogenesis is mediated by IL-6 and TNFα, two cytokines that characterize human RA inflammation,, rather than IL-17. rather than IL-17.

We noticed that while adoptively transferred Th17 cells could convert into exTh17 cells, exTh17 cells can also give rise to minimal numbers of Th17 cells. Due to the critical role of IL-17 in SKG arthritis and the reported ability of exTh17 cells to re-express IL-17 in the context of lung infection(39), we proceeded to assess whether IL-17 neutralization could reduce the pathogenic effect of exTh17 cells in SKG arthritis. Fig. 2G, H and fig. S3E-G show that while neutralization of IL-17 reduced arthritis severity and formation of exTh17 cells in Rag2-KO-Th17, it was ineffective in Rag2-KO-exTh17 mice. Insensitivity to IL-17 blockade, which is also found in chronic human RA(12), suggests that re-expression of IL-17 is an unlikely pathogenic mechanism of exTh17 cells in SKG arthritis.

Integration of bulk transcriptome and single-cell combined gene expression and chromatin accessibility data highlight subclusters of exTh17 cells that are potentially conserved in RA synovium.

Next, to dissect differences between Th17 and exTh17 cells and explore the pathogenic mechanism of exTh17 cells in SKG arthritis, we performed bulk transcriptome analysis of Th17 and exTh17 cells sorted from joints or lymph nodes of Rag2-KO-CD4 mice with chronic arthritis (day 69 to 72) (fig. S4A). The analysis of differentially expressed genes (DEseq2 adj. p-value <0.05 and TPM>5 in at least one sample) confirmed a drastic reduction of *Il17a*, *Il17f* and *Il22* in exTh17 cells compared to Th17 cells in joints and lymph nodes (Table S1). There were 158 additional downregulated genes (DEseq2 adj. p-value <0.05) in joint exTh17 cells, which had functional enrichments in inflammatory bowel disease-relevant pathways, nuclear RNA processing, and chemokine production (fig. S4B, see Table S1 for the full list of downregulated genes).

Next, we focused on the 214 genes that displayed higher expression in joint exTh17 cells vs joint Th17 cells(Fig. 3A, see Table S2 for the full list of upregulated genes). 48 of those genes were upregulated in joint exTh17 cells compared to both joint and lymph node Th17 cells. Highly expressed members of this group with known function in Th17 cells and/or inflammation are indicated by black boxes in Fig. 3B. CD44 is a well-known marker of memory T cells(40) while, *S1pr4* is one of the receptors for sphingosine-1-phosphate (S1P) and its upregulation in joint exTh17 cells was unexpected because S1P receptors are known to be downregulated in lung exTh17 cells(39). Other key exTh17 cell markers included *Rgs1*(41); *Grap2* (42), and *Gimap4* (43) (fig. S4C). Notable members of the remaining 166 genes, which were exclusively upregulated in joint exTh17 cells vs Th17 cells, included several interferon stimulated genes (ISG, Ifit3 and Ifi208) and the heat shock proteins (HSP) genes Hsph1 and Hspa1a (indicated by red boxes in Fig. 3B).

We also carried out a Gene Ontology (GO) term enrichment analysis of the 214 upregulated genes in joint exTh17 cell population and observed several GO terms and pathways (Fig. 3C,D), the most significant ones linked to cellular response to interferon-β (including several ISG), lymphocyte activation, and regulation of the NK cell response. When we compared the list of 214 genes overexpressed in joint exTh17 cell to the 347 genes which were recently found to be overexpressed in lung exTh17 cells (GSE130446)(39) we found a limited overlap consisting of only 14 genes (notably including the major ISG *Ifit3*) (fig. S4D). We conclude that a gene signature can be identified that distinguishes joint exTh17 from joint Th17 cells .

We performed single cell Multiome analysis, a combination of scRNA-seq and scATAC-seq using the 10x Genomics platform to better characterize the heterogeneity within joint exTh17 cells and to identify potential transcriptional regulatory mechanisms responsible for upregulation of signature genes. This assay, allowed us to study the trascriptional changes as well as chromatic accessibility from the same cell. (44). We obtained 8,175 joint exTh17 cells from Rag2-KO-CD4 mice with RNA-seq and ATAC-seq signals reliably measured in the same cell (median of 1242 genes and 12k fragments per cell). Utilizing our multi-modal measurements simultaneously, we performed clustering and visualized them through UMAP, highlighting 10 distinct clusters (Fig. 3E, clusters 8 and 9 with less than 100 cells were

removed from downstream analysis). To annotate these different clusters, we overlaid the UMAP with expression profiles of joint exTh17 signature genes (214 upregulated from the bulk RNA-seq) that had been previously identified . As expected, *Il17a* was almost absent from all clusters (fig. S5A). Expression of a Th17 cell signature(45) as well as of the typical Th17 cell marker CCR6 was low and mostly limited to cluster 1, while almost no expression of Cxcr3 (a marker of Th17 cell-derived Th1 cells(16)) was found (fig. S5B). Two clusters displayed enrichment with specific exTh17 cell signature genes: cluster 0 with ISG subset and cluster 3 with the HSP subset (Fig. 3E, F). These results suggested that the upregulation we detected from the bulk RNA-seq for such genes is likely a reflection of overrepresentation of cells from these specific subsets in exTh17 cells in comparison to Th17 cells. This conclusion was supported by the enrichment of a reported type 1 and type 2 IFN responsive gene signature(45) in cluster 0 (fig. S5C). We also observed that a subset of our signature genes was more widely expressed across all exTh17 cell clusters. These included *Cd44*, *S1pr4*, *Grap2* and *Rgs1*, with *Cd44* expression found at highest levels in clusters 2–4. Selective expression of genes involved in cell cycle(46) identified cluster 5 as the only proliferating one (fig. S5D) whereas the expression of an exhaustion-specific gene signature recently reported in SKG T cells (*Bach2*, *Eomes*, *Ikzf2*, *Irf4*, *Tigit*, *Tox*, *Tox2 Jun*, *Ntpd1*)(47) was weak across exTh17 cell clusters (fig. S5E).

Although exTh17 cells can only be rigorously identified in fate-mapping mouse models, given our ability to extract specific gene signatures of joint exTh17 cells that were supported by both bulk and single-cell gene expression data, we also explored whether cells with exTh17-like gene signatures could be identified among the CD4 T cells characterized from synovial biopsies of RA patients. We reanalyzed single-cell RNA-seq (scRNAseq) data from a single center cohort of five RA synovial biopsies (48) and carried out scRNAseq analysis of a new single-center cohort of 21 RA synovial biopsies (Fig. 3G, fig. S5F, Table S3). For the reanalysis, we identified the T cell cluster followed by extraction of clusters with CD4 signature leading to ~1800 $CD4^+$T cells in 6 different clusters, while the new cohort detected ~3400 CD4 T cells subdivided into 7 clusters. We assessed expression of exTh17 cell signature genes in T cells from the Accelerating Medicines Partnership (AMP) cohort(49), which consists of 52000 CD4 T cells split into 11 clusters (Fig. 3I) Quantification and visualization of exTh17 cell signature genes demonstrated that a substantial fraction of these genes was highly expressed in CD4 T cells from RA biopsies (Fig. 3HI, I, fig. S5G). As seen in mouse joint cell multiome analysis, *CD44, S1PR4, RGS1*, *GIMAP4* and *GRAP2* were expressed across all clusters for both cohorts, whereas *HSPA1A* was enriched in a clustered subset. None of the signature genes appeared to be specific to known clusters of human RA synovial CD4 T cells, however *RGS1* and *S1PR4* were enriched in Tph and Tfh, which are a key pathogenic population in human RA(50). A notable exception was that *IFIT3* displayed little if any expression in RA synovial T cells. Data from these three human cohorts show expression of key exTh17-upregulated genes in T cells from synovial biopsies of RA patients, suggesting their relevance in RA pathogenesis.

Single-cell chromatin accessibility and RNA velocity analyses highlight upstream cluster-specific regulators and potential checkpoints for exTh17 cell development.

To elucidate the upstream regulators involved in differentiation into each exTh17 cell subset/cluster, we performed motif enrichment analysis for differentially accessible regions (DARs) (Fig. 4A). Consistent with the distribution of signature genes across clusters, aggregation of scATAC-seq tracks per cluster showed cluster-specific accessibility patterns for ISG and HSP genes but not for *S1pr4* or *Cd44* (Fig. 4B). An analysis of top enriched transcription factor (TF) motifs highlighted specific patterns for clusters 0 (ISG-enriched), 3 (HSP-enriched) and 1 (low IL-17). Cluster 0 showed enrichment for the Ikaros Zinc Finger *Ikaros* (*Ikzf1*) and *Stat2*, two TF that control IFN signaling (51, 52). Binding motifs for Heat Shock Factors proteins(53) Hsf1, Hsf2 and Hsf4 which control HSP expression were distinctly enriched in cluster 3 (Fig. 4A and fig. S6A, motifs for the key enriched TF are shown in fig. S6B). Cluster 1 DARs (Fig. 4A) showed strong enrichment for TFs involved in mediating T cell activation and/or Th17 cell differentiation such as the Activator Protein-1 TF Basic leucine zipper transcription factor, ATF-like (Batf), nuclear receptor subfamily 4A (NR4A) member Nr4a1 (a.k.a. Nur77) and the two Nuclear factor of activated T-cells (NFAT) members Nfatc1 and Nfatc4(54–57). Together these data point to a potential reactivation of the Th17 cell transcriptional programs in a subset of exTh17 cells during chronic arthritis, similar to what occurs more extensively in lung exTh17 cells during an infection rechallenge(39).

We used RNA velocity analysis for insights into the potential differentiation trajectory among different subsets of joint exTh17 cells. For this, we utilized both scRNA-seq and scATAC-seq component to calculate cell velocity (Multivelo)(58). This analysis, coupled with latent time (Fig. 4C) suggested that HSP-signature cluster 3 likely represents an early differentiation state of exTh17 cells. In addition to upregulation (high velocity) and high expression of HSP genes, *Cd44* was also most upregulated in this cluster suggesting an early role for *Cd44* in exTh17 cell differentiation. Cluster 1 had low but detectable levels of *Il17a* expression and non-zero velocity for this gene, which confirmed its potential trajectory toward Th17 cell redifferentiation. The cluster with the latest latent time was cluster 0 that had both upregulation and high expression of ISG suggesting that this cluster could be a late differentiation state of exTh17 cells in mice.

FLS can modulate the joint microenvironment to promote formation of exTh17 cells.

In an attempt to localize exTh17 cells in the synovium of Rag2-KO-CD4 mice, we optimized a method for performing immunofluorescence (IF) microscopy on non-decalcified joint sections, which allows co-staining with other antibodies (Ab) while preventing the quenching of the fluorescence of tdTomato. Co-staining sections of chronically arthritic joints with anti-podoplanin (a FLS marker) and anti-IL-17 Ab showed an abundance of $Il17^{-}tdTomato^{+}$ exTh17 cells densely interspersed with FLS in the synovium, where there were very few Th17 cells (Fig. 5A and Fig. S7A). FLS-secreted IL-6 induces instability of Treg in RA and SKG synovium(30, 59). Due to the observed physical proximity of exTh17 cells to FLS, we tested whether FLS could influence the Th17-exTh17 cell conversion in an in vitro two-chamber co-culture assay. We observed that when naïve triTh17 cells were differentiated in Th17 cell polarization media(30), exTh17 cells constituted around 20% of

the resulting TdTomato$^+$ cells; however, FLS in the lower chamber led to a large increase in the fraction of resulting exTh17 cells (Fig. 5B). These experiments suggest that soluble factor(s) from FLS might play a role in promoting the conversion of Th17 cells into exTh17 cells in inflamed joints.

To gather confirmation of a potential relationship between FLS and exTh17 cells in human RA, we carried out spatial transcriptomics using the 10X Visium platform in arthroplasty human synovium from 3 RA patients (Fig. 5C-E and fig. S7B-E, Table S3). We visualized the density of transcripts that point to FLS identity (*PDPN, CDH11, PDGRFA*) and a gene signature that characterizes exTh17 cells (*CD4, CD44, S1PR4, RGS1, NKG7, LTB, IRF8, IL18R1, IFIT3, HSPH1, GRAP2, GIMAP4*). Despite the less homogeneous distribution of FLS in RA compared with SKG synovium (Fig. 5C), a co-localization analysis, using MistyR(60) showed that hot spots of that exTh17-signature tended to co-localize with hot spots of FLS in the synovial specimens analyzed (Fig. 5D,E and fig S7D,E). When we assessed the distribution of the top three pathway that differentiate mouse joint exTh17 cells versus Th17 cells (Fig. 3C), there was evidence these localized in proximity to the exTh17-FLS co-localization hot-spots (Fig. S7B). To gather further evidence at the single-cell level of co-localization between exTh17 cell markers and FLS in human RA, we subjected tissues from two synovial biopsies to spatial transcriptomic analysis using the Xenium platform(61). We used the Human Multi-Tissue and Cancer panel (377 genes) with additional custom panel of 50 genes which included FLS and exTh17 cell markers (Table S4). Fig 5F, G and Fig S7F shows that CD4 T cells with exTh17 cell markers are interspersed with fibroblasts within the synovium. A correlation analysis of exTh17 cell marker expression and proximity to FLS showed significant positive correlation for *Cd44* and *S1pr4*. These data suggest that FLS might play a role in the conversion of Th17 cells into exTh17 cells, possibly through the secretion of one or more soluble factors and/or spatial proximity between T cells and FLS.

S1pr4 contributes to joint exTh17 cell generation.

We tested multiple cytokines in an in vitro Th17 cell differentiation assay to identify which soluble factors mediate Th17 to exTh17 cell conversion. Tgfβ is a soluble factor that is produced by RA FLS(62) and is a critical promoter of exTh17-IL10$^+$ formation in colitis(37). However, addition of TGFβ to the in vitro Th17 cell differentiation assay led to a strong decrease of exTh17 cell production (Fig. 6a). Stimulation with TNFα and IL-1, cytokines that are not produced by FLS but heavily present in arthritic synovium, also did not affect the outcome of this assay (Fig. S8A). IL-7 is produced by lymphatic endothelial cells and is important for the maintenance of memory phenotype of Trm cells in the lungs(39). IL-7 is produced by FLS(63), however, neutralization of IL-7 did not reduce Th17 cell conversion in the triTh17-FLS co-culture assays (fig. S8A). The phenotype of exTh17 cells resembles cytokine-activated T cells (Tck) cells previously described in RA (64), thus we generated SKG Tck by incubating naïve SKG T cells with IL-2, IL-6 and TNFα and compared their phenotype with exTh17 cells. SKG Tck cells expressed less IL-17a and IL-6 than exTh17 cells but comparable TNF, suggesting that SKG Tck cells share some features with exTh17 cells but are not identical (fig. S8B).

FLS display abundant basal production of S1P, which is enhanced in hypoxia which can occur in the chronic RA pannus(65, 66). We repeated the triTh17 cell differentiation assay with the addition of a selective S1PR4 antagonist CYM50358(67) and noticed that the compound decreased the fraction of exTh17 cells in the assay (Fig. 6B). CYM50358 is not suited for in vivo use, so we assessed whether S1PR4 plays a role in exTh17 cell production in vivo with an in vivo knockdown strategy. TriTh17 CD4 T cells underwent in vitro CRISPR-mediated knockdown of *S1pr4* followed by transfer into Rag2-KO mice. We validated this strategy by showing that knockdown of Rorc led to a decrease in arthritis severity and differentiation of Th17 and exTh17 cells in the lymph nodes (fig S8D). Similarly, as shown in Fig. 6D-F and fig. S8C, knockdown of *S1pr4* strongly decreased the severity of arthritis and the joint exTh17/Th17 cell ratio.

We next carried out an experiment by treating Rag-KO-CD4 with the S1P inhibitor FTY720 (68, 69). Because of lack of S1P receptors on lung Trm exTh17 cells, in vivo administration of FTY720 did not affect Trm exTh17 cell numbers in the lungs(39). However, FTY720 ameliorated disease severity in several mouse models of RA including an SKG-based model(70). cellsexTh17 cell (39)Treatment with FTY720 led to a significant decrease in the severity of arthritis in Rag-KO-CD4 mice (Fig. 6G and fig. S8E). We did not detect significant changes in Th17 cell counts in the joints or lymph nodes of FTY720 treated mice however there was a strong decrease in exTh17 cell numbers in the joints with a decreasing trend also observed in the lymph nodes leading to decreased joint and lymph node exTh17/Th17 cell ratio (Fig. 6F and fig. S8F). The lymph node/joint ratio of exTh17 cells in FTY20 treated mice was much lower than for general CD4 cells or Th17 cells, pointing to substantial decrease in exTh17 cell conversion in addition to the expected lymph node sequestration (Fig.6Iand fig. S8G). To determine whether FTY20 had a specific effect on IFN-signaled T cells, we used immunofluorescence to quantify total CD3+ T cells and IFN-signaled T cells (defined by IFIT3+ CD3+ co-expression) in the joints of FTY720 vs untreated mice. We found that FTY720 reduces the total T cell number and not IFN-signaled T cells specifically (fig. S9). We conclude that signaling through the S1PR4 is likely to play a role in the conversion of Th17 cells into exTh17 cells in inflamed joints and potentially their pathogenic action in SKG arthritis. Our results also highlight that the phenotype of joint exTh17 cells is likely different from lung Trm exTh17 cells and potentially exTh17 cell populations in other tissues.

CD44 promotes the pathogenicity of exTh17 cells in inflammatory arthritis.

We used Rag2-KO-exTh17 mice to dissect the pathogenic mechanism of exTh17 cells. We focused onCD44 because of its dramatic overexpression in exTh17 cells and its known role as a promoter of arthritis in other models(71). Joint exTh17 cells produce more IL-6 and TNFα than Th17 cells. Both IL-6 and TNFα are necessary for SKG arthritis(28). Since IL-6 receptor blockade ameliorates established SKG arthritis(30), we compared the effect of global IL-6 receptor vs CD44 blockage on the severity of arthritis caused by exTh17 cells. Fig. 7A and fig. S10B show that CD44 blockade was more effective than IL-6 receptor blockade. Since CD44 is expressed in multiple cell types (including RA FLS(72)), we confirmed that in vivo CD44 knockdown reduces arthritis caused by triTh17 $CD4^+$ T cells (Fig. 7B and fig. S10A).To compare the pathogenic effect of $Cd44^+$ vs $Cd44^-$ exTh17

cells adoptively transferred into CD44$^+$ recipients, we performed in vivo knockdown *Cd44* in triTh17 cells followed by sorting of CD44$^+$ vs CD44$^-$ T cells from arthritic Rag2-KO-sgRNA_Cd44 mice and adoptive transfer of these two populations into recipient Rag2-KO mice to generate Rag2-KO-tdTomato$^+$CD44$^-$ and Rag2-KO-tdTomato$^+$CD44$^+$ mice (Fig. 7C and fig.S10C). Fig. 7D and fig. S10D shows that arthritis severity was substantially lower in Rag2-KO-tdTomato$^+$CD44$^-$ vs Rag2-KO-tdTomato$^+$CD44$^+$ mice. Flow cytometry analysis of lymph nodes (Fig. 7E, F; fig.S10E shows that the vast majority of T cells from Rag2-KO-tdTomato$^+$CD44$^-$ mice remained CD44-negative) showed increased frequency of exTh17 cells and expression of IL-6 in T cells in arthritic Rag2-KO- tdTomato$^+$CD44$^+$.

Hyaluronan is produced in large amounts by FLS(73) and CD44 has been hypothesized to mediate adhesion between lymphocytes and FLS in RA(74). CD44 is also known to enhance T cell activation(75). We hypothesized that expression of CD44 on exTh17 cells could ultimately promote FLS inflammation. We sorted joint T cells and FLS from arthritic Rag2-KO- tdTomato$^+$CD44$^-$ vs Rag2-KO- tdTomato$^+$CD44$^+$ and assessed expression of key arthritogenic genes (fig. S10F, G). As shown in Fig. 7G, CD4 cells from Rag2-KO-tdTomato$^+$CD44$^+$ displayed increased expression of *Tnfa* a key promoter of FLS inflammation(27), and FLS from Rag2-KO- tdTomato$^+$CD44$^+$ displayed increased expression of *Il6* and *Mmp3.* There was a similar, albeit not significant, trend for *Mmp2*. We conclude that overexpression of CD44 on exTh17 cells is a key promoter of the arthritogenicity of these cells, perhaps through cross talk between FLS-produced hyaluronan and CD44-mediated stimulation of proinflammatory cytokine production by exTh17 cells.

DISCUSSION

The working model suggested by our data is summarized in Fig. 7H. Overall, we show that the pro-inflammatory environment of arthritis induces a population of exTh17 cells whose phenotype is distinct from the Th1-, Tr1-, and Trm exTh17 cells described in models of colitis, EAE and lung infection(37, 39). Differentiating features of arthritis-induced exTh17 cells include persistent RORγt expression, lack of IFNγ or IL-10 expression, and the ability to promote chronicity of arthritis without re-expression of IL-17. These cells also show low proliferative features, and widespread expression of exhaustion-related genes. We show that blockage of S1P-S1PR4 signaling inhibits in vivo exTh17 cell conversion independent of the known regulation of LN T cell trafficking by S1P. This effect of S1P on exTh17 cell formation is reminiscent of the known stimulatory role of S1P on Th17 cell differentiation, which is mediated by S1PR1(76). It remains to be established whether other S1PRs play a role in exTh17 cell generation and whether S1PR4 upregulation in exTh17 cells contributes to survival or stability. We demonstrate that FLS likely play a critical role in promoting exTh17 cell generation in arthritic synovium through production of S1P. RA FLS in humans and mice express sphingosine kinases and are major producers of S1P in mouse arthritic and RA joints(77). Deletion of sphingosine kinases(65) or treatment with FTY720(78) or inhibitors of S1PR1(79) are effective in mouse models of RA.

SKG exTh17 cells have a heightened arthritogenic potential when compared to Th17 cells and promote IL-6 and TNF-enriched arthritis. As TNF is a major pro-inflammatory stimulus for FLS(27), and IL-6 promotes formation of Th17 cells, conversion of Th17 cells into

exTh17 cells might generate a vicious cycle which fuels expansion of FLS and further formation of exTh17 cells. CD44 is another molecule that is overexpressed in exTh17 cells and promotes their arthritogenicity. CD44 is highly expressed by T cells and additional cell types -including FLS- in RA synovium, and is considered as a therapeutic target for RA(71). CD44 mediates activation of T cells by hyaluronan (HA), which is highly expressed in normal and RA synovial fluid and regulates inflammation in autoimmunity(80–82). FLS are major producers of HA in RA joints(87), thus overexpression of CD44 could promote the observed physical co-localization between TNF-producing exTh17 cells and FLS. Another potential role of CD44 in exTh17-mediated pathogenesis is through its interaction with CD6, a T cell surface glycoprotein(83).

The comparative analysis of exTh17 cell transcriptional signatures and subsets from SKG vs human RA synovium enabled the identification of $CD4^+$ cells in RA synovium that share markers of SKG exTh17 cells. Expression of HSPs (which identifies cluster 3 of SKG exTh17 cells in Figs. 3, 4) might mark a subpopulation of human RA exTh17 cells. However, there was less direct correlation between the exTh17 cell clusters and CD4 clusters identified in our vs published CD4 single-cell transcriptomics studies. Human RA patient cohorts are considerably more heterogeneous than inbred mouse strains in terms of genetic structure and pathotype/FLS enrichment of synovium(84, 85) asynchronous onset of arthritis and-often- multicentric nature of the human studies. It is possible that clusters of human exTh17 cells more homologous to SKG exTh17 cells occur only in specific patients or stage of disease. For example, there is no ISG expression in T cells from established RA synovium however, Cooles et al have hypothesized that an IFN signature positivity is a feature of early RA(86). In addition, we cannot rule out that exTh17 cells are plastic and they could further morph into more RA-like CD4 clusters during the course of disease.

Our study has additional limitations. The IL-17cre driver generated by the Stockinger group (also utilized by Hirota et al(18)) inactivates expression of IL-17, thus rendering our triTh17 mice IL-17 haploinsufficient. While this might explain the slower development of arthritis displayed by triTh17 mice, triTh17 CD4+ cells were able to elicit robust arthritis after transfer into Rag2-KO mice. The dynamic appearance, distinct phenotype, and enhanced pathogenicity of exTh17 cells combined with their inability to re-express IL-17 after transfer into Rag2-KO mice strongly supports the idea that our study identified genuine exTh17 cells. Some limitations might stem from our focus on the SKG mouse model. In SKG arthritis, the role of Th17 cells and their interplay with FLS in the RA synovium has been well characterized, making it the best suited model for fate-mapping studies of Th17 cells in autoimmune arthritis. However, other aspects of human RA as less well recapitulated by the SKG model. For example, B cells albeit present in SKG synovium do not play a significant role(19, 30), while CD8 cells are found in human RA synovium(87, 88) but not in SKG synovium(30). The SKG phenotype could also be affected by the innate immune stimulus utilized to synchronize arthritis (89, 90). The assessment of synovium obtained from surgical arthroplasties carries limitations due to the frequent concurrence of pathological changes due to secondary OA.

Despite these limitations, our study does complement previous studies focused on human bona fide $IL17^{low}$ exTh17 cells. A subpopulation of IFNγ^+exTh17 cells are found in early

SKG arthritis, thus it is possible that that the reported human circulating IL17^{low} exTh17 cells represent early stage exTh17 cells. However, it is currently difficult to draw further comparisons between SKG exTh17 cells and human IL17^{low} exTh17 cells, as no genomics data is available for IL17^{low} exTh17 cells. Furthermore, the NK1.1 molecule, the murine equivalent of CD161, has not been described in mouse Th17 cells.

Our model explains previous observations that while IL-17 is necessary for triggering SKG arthritis, once disease is established, it is only mildly sensitive to IL-17 neutralization(30).Similarly, conversion of Th17 cells into exTh17 cells might in part underlie the complete absence of Th17 cells from synovia of patients with established RA -as shown now by two rounds of AMP-supported studies(15, 49)- and the consequent insensitivity of DMARD-unresponsive RA to IL-17-targeting therapies. Two recent reports on peripheral T cells from patients with pre-RA/at risk and early RA(91, 92) showed significant presence of cells with Th17 cell features in pre-RA/at risk vs patients with established RA. In patients with pre-RA/at risk, conversion of Th17 cells to exTh17 cells might contribute to loss of mucosal microbial control which is a key risk factor in the pathogenesis of RA, especially in the lung and oral mucosa (93, 94). On the other hand, IL-17 might selectively play a role in the switch from pre-RA/at risk to early RA, in which case, trials of FDA approved anti-IL-17 Ab in patients with pre-RA/at risk could delay or prevent disease.

MATERIALS AND METHODS

Study design:

The aim of this study was to investigate the presence and role of exTh17 cells in the autoimmune arthritis of the SKG mouse model and cross-correlate mouse exTh17 cell data with CD4 T cell data from human RA synovium. Our hypothesis was that Th17 cells that are present in the synovium in early arthritis can convert into exTh17 cells in the chronic phase. We utilized models of adoptive transfers of T cells from fate mapping mice and assessed human synovial specimens by single cell RNA sequencing and spatial transcriptomics. We also performed in vitro Th17 cell differentiation assays in the presence or absence of synovial fibroblasts, to examine how synovial fibroblasts in chronic arthritis may contribute to the conversion of Th17 cells into exTh17 cells. T cells for adoptive transfers were pooled from several mice, while number of recipient animals varied between 3 and 9 for each experiment. For antibody treatments, we assessed 3 recipients. For all the other experiments we assessed 4–9 recipients. These numbers were consistent with the standards described our ethical protocols, and determined to have an 80% power to see a difference with a significance of $p<0.05$. Bulk RNA sequencing studies of mouse cells were performed in 4 replicates, each one obtained by pooling cells from 7–8 mice. 10X Multiome studies were done in one experiment with a pool of 10 mice. Single cell RNAseq studies on human samples were carried out on 21 specimens. Spatial transcriptomics (ST) experiments were carried out on 5 total specimens. The robustness of the human studies was increased by either assessing our data in comparison to another independent data set or cross-correlating data between two different ST approaches (Visium platform utilized in 3 specimens and Xenium platform utilized on 2 specimens). In vitro cellular immunology experiments were

independently repeated 3–7 times, and graphing and statistical analysis were carried out on experimental replicates. No outlier removal was performed for this study. Histopathological scoring was performed blindly following Standardized Microscopic Arthritis Scoring of Histological (SMASH) guidelines (95). We have indicated in the figure legends the number of mice, or human specimens, or experimental replicates and statistical tests utilized and whether the image provided is representative of multiple replicates/experiments.

Mice.

SKG mice were obtained by Dr. S. Sakaguchi and have previously been described(19, 23, 30). Generation of C57BL/6 (B6) mice carrying the SKG mutation and the H2d MHC haplotype (B6.SKG.H2^{d}) has been previously described(22, 30). Il17a^{Cre} (Jax # 016879) (31), Il10^{eGFP} (Jax# 014530)(32), Ifng^{YFP} (Jax# 017581)(33), and B6.Cg-Gt(ROSA)26Sor$^{tm14(CAG-tdTomato)Hze}$/J floxed (R26$^{tdTomfl/fl}$; Jax# 007914)(34) mice were obtained from Jackson Laboratories (Jax) and crossed with B6.SKG.H2^{d} in house to generate B6.Il17a$^{Cre/WT}$Il10$^{eGFP/eGFP}$Ifn$\gamma^{YFP/YFP}$R26$^{tdTomfl/fl}$Zap70$^{SKG/SKG}$.H2$^{d/d}$ mice (here referred to as triTh17 cells). Rag2-knock out mice on a C57BL/6 (Jax# 008449) (96), background were crossed with congenic B6.H2^{d} (Jax # 000359) mice to generate Rag2-knock out H2^{d} mice (here referred as Rag2-KO). These mice were used as recipient of triTh17 CD4 T cells. Il17a-gfp reporter mice (C57BL/6-Il17a^{tm1Bcgen}/J [Jax# 018472(97)]) were used as source of T cells for in vitro assays. All mice were housed in the University of California San Diego (UCSD) Altman Clinical and Translational Research Institute (ACTRI), vivarium under specific pathogen–free conditions. All experiments were carried out with approval by the UCSD Institutional Animal Care and Use Committee (IACUC)–approved protocol #S16098.

Statistical analyses.

Comparisons between two groups were analyzed using unpaired t-test. All t-tests were two-tailed except for Fig S3B, which was one-tailed. Comparisons among more than two groups were analyzed using one-way ANOVA with Dunnett's post hoc test or two-way factorial ANOVA with Šídák's post hoc test. Correlation analysis was done using Pearson correlation. All statistical analyses were performed using GraphPad Prism software unless stated otherwise. The 0.05 significance level was used throughout. An independent statistician reviewed all statistics and deemed them to be appropriate.

Cell preparation and flow cytometry.

Single-cell suspensions were prepared from lymph nodes and joints (ankle and wrists). For isolation of synovial cells, joints were carefully dissected to avoid breakage of bones and bone marrow cell contamination. Joint tissue pieces were then digested at 37°C in isolation buffer containing 1 mg/ml Collagenase Type VIII (Sigma Cat# C2139–1G), 1 ug/ml DNase I (Roche Diagnostics cat#10104159001), 10% FBS, 25mM HEPES and 1% penicillin /streptomycin in RPMI 1640 medium. After isolation, cells were pre-incubated with Fc block (BD Pharmingen cat# 553142 clone 2.4G2 RUO) before antibody staining. For surface staining, fluorophore-conjugated antibodies specific for TCRβ (eF450_H57–597) and CD4 (RM4–5). For intracellular cytokine staining, cells were incubated with 20 ng/mL Phorbol 12-myristate 13-acetate (PMA, Sigma Aldrich cat# P1585) and 1 μm

Ionomycin (Sigma Aldrich cat# I0634) in the presence of Brefeldin A (1:1000 dilution, eBioscience/Thermo Fisher) for 5h at 37°. Intracellular staining was performed with the IC fixation buffer (eBioscience/Thermo Fisher) and permeabilization buffer (eBioscience/Thermo Fisher). For intracellular staining of transcription factors the FoxP3/Transcription Factor staining buffer set was used (eBioscience/Thermo Fisher). Antibodies recognizing FoxP3 (FJK-16s), RORγt (B2D), IL-17A (eBio17B7), IL-6 (MP5–20F3), and TNFa (MP6-XT22) were obtained from eBioscience/Thermo. Dead cells were excluded from analysis by staining with Fixable Viability dye from eBioscience/Thermo Fisher. Cells were analyzed on a Bio-Rad ZE5 Cell Analyzer and SONY ID7000. Flow cytometry data was analyzed using FlowJo software (Tree Star, Inc.). Gating of cells was based on isotype control and fluorochrome minus one (FMO) staining when needed. All the cells were gated on live cell population to exclude dead cells, and target population were gated on $TCR\beta^+CD4^+$ cells or $tdTomato^+CD4^+$. All the staining (surface and intracellular) were done in 96-well plate U bottom in 200ul of above-described buffers and antibody mix. For all washes, cells were transferred in 96-well V bottom plate and centrifuged for 3 minutes at 1400 rpm twice in 200ul of FACS buffer.

Isolation of CD4 T cells, Th17 and exTh17 cells for adoptive transfer experiments.

CD4 T cells were isolated from the spleen and lymph nodes of 8–10 weeks old triTh17 mice (heterozygote for the Il17a-Cre insertion) using EasySep™ Mouse $CD4^+$ T Cell Isolation Kit (StemCell Catalog #19852). After isolation, the purity and tdTomato expression in CD4 T cells was assessed by flow cytometry using a Bio-Rad ZE5 Cell Analyzer. Th17 and exTh17 cell populations were isolated for adoptive transfer into Rag2-KO from mice adoptively transferred with CD4 T cells from triTh17 mice (here referred to as Rag2-KO-CD4) using a mouse IL-17 Secretion Assay kit (Miltenyi Biotec Inc., cat# 130–094-207), a method we have previously used for the isolation of live IL-17-secreting cells (30). Briefly, a single-cell suspension was prepared from spleen and lymph nodes of arthritic Rag2-KO-CD4. Cells were stimulated with 20 ng/ml of PMA and 1 μg/ml ionomycin in TexMACS media (Miltenyi Biotec) containing 5% mouse serum for 3 hours, after which cells were stained with a streptavidin-labeled IL-17 capture reagent and incubated for 45 minutes. Cells were pre-incubated with Fc block during capture assay and before antibody staining. After stimulation, cells were counterstained with anti-biotin–APC, Viability Dye (Fixable eFluor™ 506), TCRβ (eF450_H57–597) CD4 (PE/Cy7_RM4–5). For at least 3 independent experiments, cells were stained with CD8 to check possible contamination after using CD4 T Cell Isolation Kit, and neither CD8 expression nor changing in gates were found. Before each adoptive transfer tdTomato expression in enriched $CD4^+$T cells was confirmed by flow cytometry. Th17 cells (Live $Tcrb^+CD4^+tdTomato^+IL\text{-}17A^+$) and exTh17 cells (Live $Tcrb^+CD4^+tdTomato^+$IL-17A-) cells were sorted using an FACSARIAIII or BD Aria Fusion at the Flow Cytometry core of La Jolla Institute for Immunology (LJI). For bulk RNASeq or qPCR analysis, cells were sorted directly into Trizol LS (cat# 10296010 Fisher Scientific). For adoptive transfer experiments, cells were sorted into pure FBS. For scATACSeq into PBS containing 1% BSA. Single-cell suspensions were prepared from lymph nodes and joints as described above. Dead cells were excluded, and target populations were gated on $TCR\beta^+CD4^+$ cells or $tdTomato^+CD4^+$. Flow cytometry data were analyzed using FlowJo software (Tree Star, Inc.). All the stainings (surface and intracellular) were done in 96-well

plate U bottom in 200ul of above-described buffers and antibody mix. For all washes, cells were transferred **to** 96-well V bottom plates and centrifuged for 3 minutes at 1400 rpm twice in 200ul of FACS buffer.

Adoptive transfer of CD4 T cells, Th17 and exTh17 cells to Rag2-KO mice.

triTh7 CD4 T cells (1×10^6 cells per transfer) or Th17 cells and exTh17 cells sorted from Rag2-KO-CD4 mice (1×10^5 sorted cells per transfer) were adoptively transferred into 8 to 10 weeks old Rag2-KO mice via retro-orbital (r.o.) injection. Mice adoptively transferred with Th17 or exTh17 cells are here referred to respectively as Rag2-KO-Th17 or Rag2-KO-exTh17. One week after cell transfer, arthritis was induced through a single intraperitoneal (i.p.) injection with 20 mg of mannan (Sigma-Aldrich cat# M7504), in accordance with our previously described protocol(22, 30). Arthritis was assessed as described below.

Clinical assessment of arthritis.

Arthritis was assessed in a blinded manner by clinical score and ankle thickness measurement once or twice a week. Mice were euthanized 35 to 69 days after cell transfer. Clinical signs of arthritis in front and hind paws were scored as follows (30): 0, no joint swelling; 0.1 per swollen digit joint (3 digits on front paw and 4 digits on hind paw); 0.5, mild swelling of wrist or ankle; 1.0, severe swelling of wrist or ankle. Scores for all digits, joints, wrists and ankles were combined for each mouse, yielding a maximum score of 5.4, which was considered the clinical endpoint. Ankle thickness measurement was performed with a digital caliper (Mitutoyo 700–118-20 Quick Mini Digital Thickness Gauge, Inch/Metric, with 0–12.7 mm range, 0.01 mm resolution and $^+/-0.025$ mm accuracy. Mice reaching the clinical end point score were sacrificed according to IACUC guidelines. Data were reported as the difference between measured thickness and baseline thickness for that timepoint.

Histological scoring and histomorphometry of mouse arthritic joints.

Whole joints were fixed in 10% zinc formalin for 48h, decalcified with 5% formic acid until the bones start to gain weight, trimmed, and embedded in paraffin. Sections were prepared from tissue blocks and stained with Hematoxylin Eosin (H&E) and toluidine blue (TB) at the LJI Histology Core. Joints of arthritic mice were histopathologically assessed following the Standardized Microscopic Arthritis Scoring of Histological sections 'SMASH' guidelines(95). SMASH provides standardized recommendations for processing, evaluating, and scoring histological joint sections in inflammatory arthritis models, to improve reproducibility and comparability across studies. Separate parameters are scored independently (synovial inflammation, bone erosion, cartilage damage/proteoglycan loss, possibly new bone formation). At least two non-serial sections must be blindly scored by two independent observers. Images of whole ankles or wrists were acquired using a Zeiss Axioscan.Z1 (Zeiss) slide scanner and analyzed using Zen software (Zeiss) or QuPath software (98). H&E-stained tissues were assigned a score from 0 to 4 for inflammation based on H&E staining, according to the following criteria: 0 = normal; 1 = minimal infiltration of inflammatory cells in periarticular area; 2 = mild infiltration; 3 = moderate infiltration; and 4 = marked infiltration. TB-stained tissues were assigned a score from

0 to 4 for bone resorption based on, according to the following criteria: 0 = normal; 1 = minimal (small areas of resorption, not readily apparent on low magnification); 2 = mild (more numerous areas of resorption, not readily apparent on low magnification, in trabecular or cortical bone); 3 = moderate (obvious resorption of trabecular and cortical bone, without full thickness defects in the cortex; loss of some trabeculae; lesions apparent on low magnification); and 4 = marked (full-thickness defects in the cortical bone and marked trabecular bone loss). Cartilage depletion was identified by diminished TB staining of the matrix and was scored on a scale from 0 to 4, where 0 = no cartilage destruction (full staining with TB), 1 = localized cartilage erosions, 2 = more extended cartilage erosions, 3 = severe cartilage erosions, and 4 = depletion of entire cartilage. To quantify immune cell infiltration in histological sections (Fig. S1C and Fig. S3B), representative H&E images were used to train a cell classifier using built-in classification tools to broadly classify immune cells, muscle and tendon, and bone according to recommended methods in QuPath documentation. Once trained, the classifier was then used to detect and classify types in regions of interest. Separate classifiers were trained for each histology batch analyzed. Skin and digits were excluded from the analysis to prevent misidentification of dermal cells as immune cells(99).

Treatment with neutralizing antibodies.

Rag2-KO-Th17 and/or Rag2-KO-exTh17 mice were injected with either IL-17A neutralizing antibody (100μg, BioXcell, Clone 17F3), anti–IL-6R blocking antibody (200μg, BioXcell, Clone 15A7), a CD44 blocking antibody (150μg, BioXcell, Clone M7) or an IgG isotype control (BIoXcell, Clone MOPC-21). The first antibody administration was done r.o. 2 hours before the i.p. injection with mannan. Subsequent antibody administrations were done via i.p injections once per week for a total of 4 weeks. All antibodies were diluted in sterile PBS.

qPCR analysis.

Sorted cells (T cells or subsets, myeloid cells, and fibroblast) were directly sorted in TRIzol LS. For whole mouse joints, flash frozen samples were first smashed then homogenated in TRIzol (cat# 15596018 Invitrogen) on ice using a hand homogenizer. CD4 T cells from triTh17 cells after CRISPR-Cas9 cell culture were directly lysed in RLT^{+}10% β-Mercaptoethanol (cat# 74034 Qiagen and Sigma Aldrich cat# M3148) lysing buffer. RNA was purified from the chloroform phase or RTL^{+} β - Mercaptoethanol lysing buffer using the RNAeasy Plus Micro kit (cat# 74034 Qiagen). cDNA was synthesized using the SuperScript III First-Strand Synthesis SuperMix for real-time quantitative reverse transcription PCR (cat# 11752250 Life Technologies). qPCR was performed on a Bio-Rad CFX384 Real-Time PCR Detection System, with primer assays (Sigma Aldrich cat #KSPQ12012G) in a final concentration of 10μM and SYBR Green qPCR Master Mix from Qiagen (cat# 330513). Primer assay efficiencies were guaranteed by the manufacturer to be greater than 90%. Each reaction was carried out in technical triplicates, and data were normalized to the expression levels of the housekeeping gene G*apdh*. Results are presented as fold change compared to the expression level in control samples with the Relative Quantification (RQ) method compared to the expression of *Gapdh.* Gene list with RefSeq IDs: *Cxcl13* (NM_018866),

Il17a (NM_010552), *Il6* (NM_031168), *Mmp2* (NM_008610), *Mmp3* (NM_010809), *Rorc* (NM_011281), *Tnf* (NM_013693), *Gapdh* (NM_008085).

Bulk RNA sequencing.

Experiment. Th17 and exTh17 cells from pooled lymph nodes and joints of 6–8 arthritic Rag2-KO-CD4 were subjected to the above-described IL-17 capture assay and sorted in Trizol LS. SMARTer® Stranded Total RNA-Seq Kit v2 was used for low input RNA (cat# 634411). Sequencing was performed at the Next Generation Sequencing Core of LJI. Quantification of gene expression. RNA-seq data was processed by our custom pipeline (https://github.com/ay-lab/RNA_SEQ_PIPELINE, https://doi.org/10.5281/zenodo.17317028). Input fastq files were processed by *fastp* for QC analysis (100). Paired-end RNA-seq reads were aligned with respect to the mm10 reference genome using the default parameters of STAR (version 2.7.3a) (101). GENCODE v23 GTF annotation file was used as reference. STAR *quantMode geneCounts* was used to estimate the gene counts. Differential gene expression analysis. The raw gene counts from individual samples were used with DESeq2(102) (version 1.34.0) to identify differentially expressed (DE) genes. P-values for differential expression were calculated using the Wald test for differences between the base means of two conditions. These p-values were then adjusted for multiple testing using the Benjamini-Hochberg method. We considered genes differentially expressed between two groups of samples when the DESeq2 analysis resulted in an adjusted $P < 0.05$ and the gene had expression > 5 TPM for at least one input sample. Pathway analysis. The analysis was done with online version of Metascape(103) on the 214 upregulated DE genes in Joint_exTh17. All terms with statistically significant enrichments were then hierarchically clustered based on similarities among their gene sets. In Fig. 3d we selected a subset of representative terms from each cluster and converted them into a network layout using Cytoscape(104) with “force-directed” layout and with edge bundled for clarity. Each term is represented by a circle node, where its size is proportional to the number of input genes fall under that term, and its color represents cluster identity. Terms with a similarity score > 0.3 are linked by an edge (the thickness of the edge represents the similarity score). One term from each cluster is selected to have its description shown as label.

10x Multiome (scRNA-seq + scATAC-seq) sequencing.

Experiment. Th17 and exTh17 cells from pooled lymph nodes and joints of 6 arthritic Rag2-KO-CD4 were subjected to the above-described IL-17 capture assay and sorted. scRNA-seq + scATAC-seq (10x Multiome) was performed at the LJI Next Generation Sequencing core facility using Chromium Next GEM Single Cell Multiome ATAC+ Gene Expression kit (10X Genomics cat#1000283). 10x Multiome cell cluster analysis. We processed the Multiome datasets using cellranger-arc (version 2.0.1) routines *mkfastq*, *count* and *aggr*, with respect to the reference genome mm10. The cellranger-arc output gene expression matrices and chromatin accessibility fragment files were then exported to Signac (version 1.6.0) (105). We used mm10 reference genome and EnsDb.Mmusculus.v79 annotation in Signac. To remove any low-quality cells, we only retained the cells having RNA count between 1000 and 25,000, and ATAC count between 1000 and 100,000, nucleosome signal < 2 and TSS enrichment > 1. We also removed any ATAC-seq signal from non-standard chromosomes, and inferred the ATAC-seq peaks by MACS2 (106). Gene expression (RNA)

was normalized using the routine *SCTransform*, and PCA was used for dimensionality reduction. ATAC-seq data was normalized by the routines *RunTFIDF* and *RunSVD*. Feature reduction in ATAC-seq was done using latent semantic indexing (LSI). Finally, the clustering was performed on the multimodal data (assay SCT) using the weighted nearest neighbor (WNN) algorithm, dimensionality reductions with PCA (dimensions 1:50) and LSI (dimensions 2:40), and employing the resolution 0.3. UMAP was used to visualize the clusters. Cluster-specific upregulated peaks were identified using the function *FindMarkers* with logistic regression (LR) test. scATAC-seq motif analysis. Cluster-wise ATAC-seq signal coverages were plotted using the routine *CoveragePlot* of Signac. We used JASPAR2020 core motifs (genome mm10) for motif analysis. First, we extracted top differentially accessible peaks (p-value < 0.005) from each cluster and applied the Signac function *FindMotifs* to identify the motifs enriched in cluster-specific topmost differentially accessible peaks. Union of top 5 significant motifs from each cluster were used to plot (R *balloonplot*) the cluster-specific motif enrichment and the percentage of cells expressing these motifs. Identification of peak-to-gene links was performed by the Signac routine *LinkPeaks*. Co-accessibility analysis was performed by Cicero, using the Signac routines *make_cicero_cds* and *run_cicero*. Gene signature analysis for single cells. For each literature-derived gene set of interest, we used the AddModuleScore() routine of Seurat to perform the gene set signature analysis. We used scaled normalized gene expression data as the input. For this analysis, Seurat first computes average expression for each gene across all cells, sorts the genes with respect to this average expression and distributes them into equally sized bins called expression bins (nbin=24 by default) with each bin including genes with similar average expression. Next, for each gene in the signature gene set of interest, it samples a number of control genes (we used ctrl=5) from the expression bin that the specific gene of interest falls in. The mean of expression differences between the signature genes and the sampled control genes determines the signature score with positive values indicating higher mean expression for that cell for the signature gene set compared to the matching control set. Signature gene sets for type I and II IFN signaling was derived from Seumois et al., 2020(45), for cell cycle from Best et al., 2013(46), for anergy and exhaustion from Ashouri et al., 2022(47) and for Trm from Amezcua Vesely et al., 2019(39).

Human scRNA-seq data analysis.

The first human scRNA-seq data used in this study was downloaded from the NCBI Sequence Read Archive (SRA) database accession code PRJNA725073(48). We used cell ranger-count (version 3.0.2) and reference genome GRCh38 to align the fastq files. We then used Seurat (version 4.0.2) functions *read10X* and *merge* to combine the gene expression matrices from cell ranger into one Seurat object. All cells were removed that had either more than 20,000 UMIs, over 5000 or below 500 expressed genes, or over 20% UMIs derived from mitochondrial genome. The transcriptome data was log-transformed and normalized by a factor of 10,000 per cell. Principal component analysis was carried out using the top 2000 variable genes on scaled counts. To eliminate any batch effects, we used the *RunHarmony* function from the package Harmony(107). Seurat clustering was performed using Louvain algorithm with resolution = 0.5, and clusters were visualized using UMAP. We annotated the T cell clusters using the marker genes provided in the Supplementary Table 4 (15). We then re-clustered the extracted T cells using the same clustering parameters

and identified the CD4 and CD8 cell types using the marker genes provided in the same document. Finally, we extracted the cells corresponding to CD4 T cells, and re-clustered them using the same clustering parameters. The second human scRNA-seq data used in this study was performed at Northwestern University. We recruited DMARD-naïve RA patients that have a diagnosis of RA as defined by either the 1987 ACR (108) or 2010 ACR criteria (109), ages 18–80 years with adult-onset RA who have at least moderately active disease, defined as a Simplified Disease Activity Index (SDAI) >11.0, at least 4 swollen joints at screening and are DMARD naive. We defined DMARD-naïve as patients who have not received any DMARD but have been treated with NSAIDs and/or acute steroid treatment. In addition, all patients must have at least one inflamed joint (knee, wrist, elbow, ankle) that meets the ultrasound criteria for active disease, which is at least a grey scale of 2 or greater (110). The exclusion criteria was (1) Pregnant or lactating women, (2) Active infections, (3) Uncontrolled renal, hepatic, hematologic, gastrointestinal, endocrine, pulmonary, cardiac, or neurologic disease, (4) History of bleeding disorder, (4) Platelet count (within one month of biopsy) less than 100×10^3 cells/mL, (5) History of infection with human immunodeficiency virus (HIV), hepatitis B, or hepatitis C, (6) Documented diagnosis of SLE or seronegative spondyloarthropathy, (7) Soft tissue or intra-muscular corticosteroid injections within 4 weeks prior to biopsy, (8) Corticosteroid injection in joint to be biopsied within 8 weeks prior to biopsy, (9) Current use of warfarin, clopidogrel, or other anticoagulant, (10) Prednisone dose > 10 mg daily and (11) any DMARD. The synovial biopsy was performed as we described (111), consistent with all published studies using ultrasound guided synovial biopsies (110, 112–125) on wrist or knee. Previous studies have shown that paired wrist and knee biopsies exhibit similar histologic features (126). Human samples were processed as previously described (111) and in agreement with SOPs developed by the AMP consortium (127). We performed CITE-seq on $CD45^+$-sorted cells on the same day as the biopsy. Single-cell samples were processed in metabolomics core at Northwestern University. The Next Generation Sequencing (NGS) facility at Northwestern University performed quality control (QC) by Tapestation, and samples were sequence on an Illumina Nova seq machine. Before full sequencing, we performed MiniSeq runs to ensure the quality of samples and estimate cell numbers for more accurate sequencing depth. Sequenced libraries were processed using the CellRanger pipeline to generate the single-cell matrix files of RNA and ADT. Sequencing metrics, including alignment, read quality, fraction of reads in cells, and detected genes, were assessed for sample QC. The Seurat R package was used to perform filtering of cells for potential doublets, empty droplets, and high percent mitochondrial reads. Seurat and/or Harmony was used to merge samples across patients and initial analysis of RNA data including clustering, visualization, and annotation. We then extracted the cells corresponding to CD4 T cells, and re-clustered them for further analysis.

RNA Velocity analysis using MultiVelo.

RNA velocity analysis on multi-omics data was performed by MultiVelo(58). First, gene expression matrices from Cell Ranger ARC were converted to MultiVelo compatible loom format using the tool Velocyto(128). In addition, we provided the ATAC-seq peak annotation file (atac_peak_annotation.tsv) and feature linkage file (feature_linkage.bedpe) from cell ranger-arc output as the inputs to MultiVelo. We also extracted the neighborhood graph

information from Signac object, together with its UMAP coordinates, as the inputs to MultiVelo, so as to use the UMAP embedding computed in Signac, instead of re-computing them in MultiVelo. We followed the MultiVelo documentation to process the input RNA and ATAC files, integrate ATAC peaks, normalize the peaks using TF-IDF, and integrate both omics data. We used the *recover_dynamics_chrom* routine in MultiVelo to run the multi-omics dynamical model, and computed velocity stream and latent time using the routines *velocity_graph* and *latent_time*, respectively. The routine *velocity_embedding_stream* in MultiVelo was used to generate the stream plot of velocity, while the functions *pl.scatter* and *pl.velocity* from scVelo(129) were employed to plot the variation of latent time, velocity and gene expression.

Gene regulatory network analysis.

Gene regulatory network using the multi-omics data was inferred by SCENIC$^+$ pipeline [Scenicplus2022](130). We skipped the scRNA-seq UMAP and clustering in SCENIC$^+$, and re-used the UMAP coordinates and clustering outputs from Signac. We followed the SCENIC$^+$ tutorial to process the ATAC-seq component using *cisTopic*. We provided the cell barcodes from the input Signac object to the *valid_bc* argument of function *create_cistopic*_object_from_*fragments* to ensure that the same cells from Signac object were used in the cisTopic object instead of using the QC-filtered cell barcodes from SCENIC$^+$. We followed the SCENIC$^+$ pipeline for analyzing motif enrichment and generating eRegulons. From the filtered eRegulons (generated by the pipeline), we considered only those TFs for network analysis which regulate one or more differentially expressed genes derived from bulk RNA-seq data.

Confocal microscopy.

Ankles from arthritic Rag2-KO-CD4 mice were harvested and fixed for 8–10h in 4% paraformaldehyde (PFA) at room temperature. After fixation, samples were washed twice with PBS and transferred into 30% sucrose overnight at 4°C followed by two more washes and buffer replacement then diluted 1:1 into a solution of 50% Optimal Cutting Temperature compound (OCT, Sakura cat#4583) and 30% sucrose (reaching a final concentration of 25% OCT and 15% sucrose) Samples were processed at the LJI Histology and Microscopy core without decalcification. Ankles were embedded in OCT and 4 μm sections were cut with a CryoJane Tape-Transfer System (Leica BioSystem cat#39475205). Before staining, the sections were air dried to promote tissue adhesion and blocked using a 10% normal goat serum (Cat# G9023–10mL Sigma Aldrich), 0.5% BSA blocking solution (Cat# 10735078001 Roche) and 1:100 Fc block (Cat# 101302 BioLegend). Slides were stained for podoplanin (primary antibody Cat# 14–5381-82 Thermo Scientific, 1:800 dilution) or CD4 (primary antibody Cat# 14–0042-82 Thermo Scientific, 1:100 dilution) with Alexa Fluor 594 (secondary antibody cat# A-21113 Thermo Scientific, 1:500 dilution), or IL-17A (primary antibody cat# PA5–106856 Thermo Scientific, 1:400 dilution) with Alexa Fluor 647 (secondary antibody cat# A32733 Thermo Scientific, 1:500 dilution) and Hoechst 3342 (Cat# H3570 Thermo Scientific, 1:1000 dilution). Some slides were stained for Il17 as above and for CD4 (Fig. S7A). Whole slides were imaged for the above listed fluorophores and tdTomato expressed by the transferred T cells with Zeiss AxioScan Z1 (20× 0.8NA, Colibri 7 light source, Hamamatsu OrcaFlash 4.0 camera, and appropriate single-band filter cubes).

Regions of interest were further analyzed using a Zeiss LSM 880 microscope. We used a 40× 1.4NA oil objective, 405, 561, 594, 633 nm excitation, spectral detection ranges set up using single-stained controls (415–695 nm, 561–588 nm, 606–668 nm, and 662–721 nm, respectively). Voxel size was set to 60×60×450 nm, pixel dwell time was 1.22 μs, and 15 Z slices encompassing tissue thickness were max intensity projected in ZEN software. Images were further analyzed with QuPath.

Preparation of mouse FLS lines.

Ankle joints from 8 to 10-weeks-old C57BL/6 (B6) mice were isolated. Briefly, minced tissues were digested in collagenase IV (0.5 mg/ml) (Sigma cat#C2139) in RPMI 1640 (Gibco cat#11875093) for 2 hours at 37°C with gentle agitation and the cultured in complete Dulbecco's modified Eagle's medium (Corning cat#10–017-CV) (21). For all experiments, FLS were used between passages 4 and 8.

CD4 T cell-mFLS co-culture assay.

Naïve CD4 cells were isolated from 10–14 weeks old triTh17 mice using EasySep™ Mouse Naïve $CD4^+$ T Cell Isolation Kit (cat# 19765). 2–3.5 $\times 10^5$ cells were cultured in anti-CD3 coated (2μg/ml, clone 145–2C11, cat# 10030 Biolegend) 12 or 24 well plates under Th17 cell polarization conditions - T cells media with: 50 ng/mL IL-6 (cat# 406-ML-005 R&D Systems), 5 ng/mL rhTgfb (cat# 240-B-002 R&D Systems), 1 ug/mL LEAF anti-CD28 (clone 37.51 cat# 102115 Biolegend), 10 ug/mL Ultra-LEAF anti-IL-4 (clone: 11B11, Cat# 504121 Biolegend), 10 ug/mL Ultra-LEAF anti-IFNγ (clone: XMG1.2, cat# 505705 Biolegend), 10 ug/mL Leaf anti-IL-2 Biolegend (Clone: JES6–1A12, Cat# 503704 Biolegend). Anti-CD3 coating was done for 3h at 37°C or overnight at 4°C and plates were washed once with PBS before naïve CD4 cell seeding. Naïve CD4 were cultured under polarization conditions for 5 days with and without CYM50358 (Sigma Aldrich cat# 567737) with final concentration of 25nM. Mature Th17 cells were cultured for 3 days with 20ng/ml of IL-2 (R&D cat# 402-ML-100/CF) and 10μl/1$\times 10^6$cells of mouse T-Activator (Thermo Fisher Dynabeads™ Mouse T-Activator CD3/CD28 for T Cell Expansion and Activation cat# 11456D). For mFLS co-culture assays, mFLS were kept separated from naïve CD4 T cells by a 0.4 um pore polyester membrane (Corning Cat# 3470). Naïve CD4 T were cultured in an anti-CD3 coated plate and 2–3$\times 10^4$ mFLS were equilibrated overnight (day 0) in the transwell with complete T cell media before the co-culture with naïve CD4 T cells. At the time of co-culture with mFLS (day 1) naïve CD4 T cells were plated the anti-CD3 coated plate, complete T cell media was removed from mFLS and replaced with Th17 cell polarization media. Both cell type mFLS and naïve CD4 T cells were cultured under Th17 cell polarization media. After 5 days, T cells were harvested, washed twice with PBS, and stimulated with 20 ng/mL PMA and 1 μm ionomycin and 1x brefeldin A in complete T cell media for 4–5h at 37°C before analysis. All the stainings (surface and intracellular) were done in 96-well U bottom plates in 200ul of the above-described buffers and antibody mix. For all washes cells were transferred in 96-well V bottom plates and centrifuged for 3 minutes at 1400 rpm twice in 200ul of FACS buffer.

Spatial Transcriptomics 10X Visium on FF Human Synovium.

Experiment. Human synovium samples from total hip arthroplasties of patient diagnosed with RA according to 1987(108) or 2010(109) criteria were obtained from the Pini Orthopedic Hospital (a teaching hospital of University of Milan) in Italy. The study was approved by the local ethical committee (Comitato Etico Milano Area 2, RF-2018–465_2017bis/963_2019) which was submitted to and ratified by the UCSD IRB. Clinical data about the patients are shown in Supplementary Table 1. The synovium was collected during the surgery and immediately embedded in OCT, flash frozen and stored at −80°C then processed at the LJI Histology and Microscopy core. Prior experiment, 3 μm section were cut from the OCT blocks and subjected to a tissue optimization (TO) assay to select the ideal permeabilization time needed to release RNA from the tissue to the slide. During this step cDNA staining was performed in the time of RT (Reverse Transcriptase) reaction. Fluorescent cDNA tissue (on the tissue permeabilization slide) was imaged with Zeiss Axioscan.Z1 (Zeiss) slide scanner to determinate the ideal permeabilization time. Entire TO experiment was done following 10X Genomics protocols. For gene expression experiment, 3 μm section were cut from the OCT blocks and placed on the Visium Spatial Gene Expression slide inside the 6.5 × 6.5mm fiducial frame. The area inside the fiducial frame contains 5000 barcoded spots. Tissues were fixed and stained with H&E according with 10X Genomics protocols prior to imaging. The GEX slide was H&E stained and imaged at 10X and 20X magnification on an Axioscan.Z1 (Zeiss) slide scanner. The percentage of tissue within the fiducial frame was measured using the tissue recognition tool on QuPath software and sequencing depth was calculated accordingly. Sequencing was performed at the LJI Next Generation Sequencing core. Cell clustering and MistyR analysis . Raw sequencing data was demultiplexed and converted to fastq format by using bcl2fastq v2.20 (Illumina). Space Ranger software v2.0.0 (10X Genomics) was used for reads alignment, tissue detection, fiducial detection, and barcode/UMI counting with default parameter. Briefly, raw reads were aligned to the human reference transcriptome (GRCh38, version=2020-A), then reads with the same barcode, UMI and gene annotation were grouped for UMI counting. For image processing, the slides' barcoded spot pattern was aligned to the input image, and tissue and background were discriminated. A UMI count matrix was generated, with gene identities as rows and spatial barcodes as columns. Seurat v4.2.1(131) in R v4.1.3 was used for advanced downstream analysis. The matrix was loaded into Seurat to create a Seurat object and low-quality spots were filtered out based on the total number of UMI (< 600 and > 30,000) and total number of genes expressed (< 300). Further, spots with > 15% reads mapped to mitochondrial genes were removed. Count data of the remained spots was normalized using sctransform(132). To obtain two-dimensional projections of the population's dynamics, principal component analysis (PCA) was run on the top 5,000 most variable genes to reduce the number of features. The top 5,000 most variable genes were identified based on their mean and dispersion. After running PCA, t-distributed stochastic neighbor embedding (t-SNE) analysis was performed to further reduce these components to visualize spots in a two-dimensional space. SPATA2(133) was used to calculate the average expression of exTh17 cell and FLS marker genes. MistyR (v1.6.0)(60) was used to investigate the associations between the exTh17 cell and FLS maker genes. In MistyR, the neighborhood parameter was set to 5 spots and the cutoff threshold for the importance scores of markers was set to 0.5 standard deviation.

In situ gene expression analysis by Xenium

Synovial biopsies were prepared following the manufacturer's protocol (10X Genomics, CG000578 Xenium In Situ for FFPE Tissue Preparation Guide) at the Northwestern core facility. Formalin-Fixed Paraffin-Embedded (FFPE) tissues were sectioned at 5 μm thickness, placed onto Xenium slides, and underwent deparaffinization and decrosslinking (CG000580) to expose RNA targets. A pre-designed panel from Xenium (377 genes on the Human Multi-Tissue and Cancer Panel) and an Add-on custom design panel (50 genes) (Supplementary Table 4) were used. Gene expression detection involved probe hybridization (CG000749) at 50°C overnight, followed by washing, ligation, and rolling circle amplification (RCA) to amplify the signal. Samples were subsequently blocked and stained at 4°C overnight. Autofluorescence was chemically quenched, and nuclei were stained with DAPI before imaging. The prepared slides were analyzed using the Xenium Analyzer (10X Genomics), running on Instrument Software Version 3.0.2.0 with Analysis Version xenium-3.0.0.15. We used two regions (region 3 and region 4) of the Xenium slide for downstream analysis. For cell segmentation, DAPI-stained nuclei from the DAPI morphology image were segmented to define individual cells. Nuclear boundaries were either expanded or combined with a cell boundary stain, ensuring accurate transcript assignment per cell. Cell segmentation was performed with 10X Xenium onboard cell segmentation. For each sample, count matrices were generated based on the expression of transcriptomics inside each segmented cell along with x and y coordinates. Scanpy v1.9.3 was used for downstream analysis. For quality control all cells with $n < 50$ total transcripts for region 3 and $n < 25$ total transcripts for region 4 were filtered out before downstream processing. Count data of the remained cells were log-normalized. Dimensionality reduction was performed with principal component analysis (PCA). Marker genes for exTh17 cells and Fibroblasts were used for cell type annotation (Fig. 5G). To investigate the role of FLS in exTh17 cell generation, neighborhood analysis was performed by calculating the correlation between the expression levels of CD44 and S1PR4 in exTh17 cells and their distances to the closest FLS cells (Fig. 5H). The results show that exTh17 cells near FLS cells express higher levels of CD44 and S1PR4. Negative correlation values indicate that as the distance from exTh17 cells to the nearest FLS cells increases, the expression levels of CD44 and S1PR4 decreases.

In vivo CRISPR-Cas9 gene knockdown.

$CD4^+$ T cells from 8–10 weeks old triTh17 mice were isolated using the EasySep™ Mouse CD4 T Cell Isolation Kit. After isolation, cells were cultured for 3 days with 20ng/ml of IL-2 and 10 μl/1×10^6 cells of mouse anti-CD3/CD28 coated beads Activator. Following expansion, 1×10^6 - 2×10^6 cells per condition were nucleofected with 0.65 μM of Cas9 Nuclease (IDT Alt-R® S.p. HiFi Cas9 Nuclease V3, 500 μg cat# 189676867) and single guide RNA (sgRNA) against CD44 (cat# SQ-041132–01-0002), S1pr4 (cat# SQ-044703–01- 0002) or control (cat# U-009505–01-02). All single guide RNA were bought from Horizon Discovery Biosciences. After nucleofection, cells were cultured for 3 h in complete T cells media, after which mouse IL-2 (20ng/ml) and anti-CD3/CD28 coated beads were added to the media and cells were cultured for an additional 2 days. After 2 days, the anti-CD3/CD28 coated beads were removed from the cells and small aliquots were stored for assessment of knockdown by qPCR. The remaining cells were adoptively transferred to 8–

10 weeks old Rag2-KO mice (3×10^5 cells per mouse). One week after transfer, arthritis was induced one week after transfer through an i.p. injection of mannan (20 mg) and assessed as described above. Mice transferred with CD4 T cells nucleofected with CD44, S1pr4, or control sgRNA are referred to as Rag2-KO-sgRNA_CD44, Rag2-KO-sgRNA_S1pr4 and Rag2-KO-sgRNA_Ctrl, respectively. All the staining (surface and intracellular) were done in 96-well plate U bottom in 200ul of above-described buffers and antibody mix. For all the washes cells were transferred in 96-well V bottom plate and centrifuged for 3 minutes at 1400 rpm twice in 200ul of FACS buffer.

Treatment of mice with FTY720.

Rag2-KO were adoptively transferred with $CD4^{+=}$ T cells from triTh17 mice as described above. One week after transfer, Rag2-KO-CD4 mice were injected with mannan (20 mg) to induce arthritis and 1mg/Kg of FTY720 (Tocris Biotecne cat# 6176) was administered by oral gavage every other day for a total of 35 days(70).

$tdTomato^+CD44^-$ vs $tdTomato^+CD44^+$ adoptive transfers.

$CD4^+$T cells were isolated from triTh17 mice and nucleofected with sgRNA targeting CD44 as described above. Nucleofected T cells were adoptively transferred into Rag2-KO mice and arthritis was induced one week after transfer through an i.p. injection of mannan (20 mg). At day 52, $tdTomato^+CD44^-$ and $tdTomato^+CD44^+$ $CD4^+$ T cells were flow sorted from lymph nodes of arthritic Rag2-KO-sgRNA_CD44 mice (Fig. S10C). Flow sorted $tdTomato^+$CD44- and $tdTomato^+CD44^+$ cells (1×10^5 per mouse) were then adoptively transferred into new recipient Rag2-KO mice and arthritis was induced one week after transfer through an i.p. injection of mannan (20 mg) and assessed as described above. At day 49, $CD4^+$ T cells subsets in lymph nodes and joints were analyzed by flow cytometry. Fibroblast ($CD90^+$CD31-CD45-) and T cells ($CD45^+TCRb^+$CD11b-) cells were flow sorted (Fig. S10F,G) from the joints of arthritic mice for gene expression analysis by qPCR (2 mice were pooled to obtain enough mRNA, which was then quantified in technical triplicates).

Immunofluorescence staining of CD3 and IFIT3 on FFPE mouse joints.

Wrists from arthritic Rag2-KO-CD4 mice were harvested, fixed, decalcified and paraffin-embedded as previously described. Before staining, the sections were air dried to promote tissue adhesion and baked at 60°C overnight. Following deparaffinization and rehydration, antigen retrieval was performed by steaming slides for 20 minutes in 1X citrate buffer pH 6 (Cat# ab64236 Abcam). Sections were permeabilized in 0.2% Triton in PBS for 10 minutes and blocked with 5% BSA blocking solution (Cat# 50–550-390 Fisher). Sections were stained for CD3 (primary antibody Cat# MCA1477 BioRad, 1:100 dilution) with Alexa Fluor 647 (secondary antibody cat# A-21247 Thermo Scientific, 1:1000 dilution), and IFIT3 (primary antibody cat# PA5–22230 Thermo Scientific, 1:50 dilution) with Alexa Fluor 568 (secondary antibody cat# A-11011 Thermo Scientific, 1:1000 dilution) and Hoechst 33342 (Cat# 62249 Thermo Scientific, 1:1000 dilution). Slides were imaged for the above listed fluorophores with ECHO Revolve Microscope (ECHO Revolve, and appropriate single-band filter cubes). Photos were taken with 40x oil objective, 380, 560, 630 nm excitation. Regions of interest were defined as a field of view with at least one CD3+ cell. 5 photos of regions

of interest were taken per section. Photos were randomized in ImageJ (Fiji) and counting of CD3 positive and IFIT3 and CD3 double positive cells was done blinded.

Tck assay.

Naïve CD4 cells were isolated from 8–10 weeks old SKG mice using EasySep™ Mouse Naïve CD4+ T Cell Isolation Kit (cat# 19765 StemCell Technologies). 2 $\times 10^5$ cells were cultured in anti-CD3 coated (2μg/ml, clone 145–2C11, cat# 10030 Biolegend) 96 well plates under Th17 cell polarization conditions - T cells media with: 50 ng/mL IL-6 (cat# 406-ML-005 R&D Systems), 5 ng/mL rhTgfb (cat# 240-B-002 R&D Systems), 1 ug/mL LEAF anti-CD28 (clone 37.51 cat# 102115 Biolegend), 10 ug/mL Ultra-LEAF anti-IL-4 (clone: 11B11, Cat# 504121 Biolegend), 10 ug/mL Ultra-LEAF anti-IFNγ (clone: XMG1.2, cat# 505705 Biolegend), 10 ug/mL Leaf anti-IL-2 Biolegend (Clone: JES6–1A12, Cat# 503704 Biolegend). Anti-CD3 coating was done for 3h at 37°C or overnight at 4°C and plates were washed once with PBS before naïve CD4 cell seeding. On day1, naive CD4 were restimulated with T cells media with: 50 ng/mL IL-6, 5 ng/mL rhTgfb, 1 ug/mL LEAF anti-CD28 in anti-CD3 coated plate, On day4, mature Th17 cells were washed with T cells media and cultured under two different condition: Th17 cell condition - T cells media with: 50 ng/mL IL-6, 5 ng/mL rhTgfb, 1 ug/mL LEAF anti-CD28 in anti-CD3 coated plate or Tck condition - T cells media with: 100 ng/mL IL-6, 25 ng/mL IL-2, 25 ng/mL TNF-α (cat# 130–101-688 Miltenyi Biotec), 1 ug/mL LEAF anti-CD28 in anti-CD3 coated plate. After 3 days, T cells were harvested, washed twice with PBS, and stimulated with 20 ng/mL PMA and 1 μm Ionomycin and 1x Brefeldin A in complete T cell media for 4–5h at 37°C before analysis. All the stainings (surface and intracellular) were done in 96-well plate U bottom in 200ul of the above-described buffers and antibody mix. For all the washes cells were transferred in 96-well V bottom plate and centrifuged for 3 minutes at 1400 rpm twice in 200ul of FACS buffer.

Supplementary Material

Refer to Web version on PubMed Central for supplementary material.

ACKNOWLEDGEMENTS:

We thank all the members of the Bottini laboratory for useful data discussion and acknowledge the precious help of expert personnel at the Biostatistics Shared Resource at Cedars-Sinai (J. Mirocha), LJI Next Generation Sequencing (S. Alarcon, H. Dose), Flow Cytometry Core (C. Kim, D. Hinz, C. Dillingham) and Microscopy and Histology Core Facilities.

Funding:

Supported by UCSD and CSMC Institutional funds and NIH grant R21 AI154964 and R01 AR066053 to N.B., a joint LJI-UCSD pilot grant (to N.B. and F.A.) and LJI Institutional Funds (F.A.). A.S. is funded by NIH T32 HL170963. We wish to acknowledge support by the following NIH S10 instrumentation grants awarded to LJI: OD021831 (Zeiss LSM 880 microscope); RR027366 (FACSAria II Cell Sorter); OD025052 (NovaSeq 6000). The human RA tissue collection was supported by the Italian Ministry of Health grant RF-2018–12365439 to F.I. and P.S.R.

Data and materials availability:

SKG Mice are available upon request. Mouse bulk RNA-seq and scRNA-seq + scATAC-seq (10x Multiome) data are available through GEO Accession ID GSE234597. Human synovial Visium data is available through GEO Accession ID GSE232734. Human synovial scRNA-seq (Hu2) data is available through GEO Accession ID GSE303539. Human synovial Xenium data is available through GEO Accession ID GSE293972. Computer code can be accessed at the following links: https://github.com/ay-lab/RNA_SEQ_PIPELINE, https://doi.org/10.5281/zenodo.17317028. All other data needed to support the conclusions of the paper are present in the paper or the Supplementary Materials. Tabulated data underlying Figs. 1 to 7 and figs. S1 to S10 are provided in data file S1. All data are available in the main text or the supplementary materials.

REFERENCES

1. Schnell A, Littman DR, Kuchroo VK, T(H)17 cell heterogeneity and its role in tissue inflammation. Nat Immunol 24, 19–29 (2023). [PubMed: 36596896]
2. Harrington LE, Hatton RD, Mangan PR, Turner H, Murphy TL, Murphy KM, Weaver CT, Interleukin 17-producing CD4+ effector T cells develop via a lineage distinct from the T helper type 1 and 2 lineages. Nat Immunol 6, 1123–1132 (2005). [PubMed: 16200070]
3. Langrish CL, Chen Y, Blumenschein WM, Mattson J, Basham B, Sedgwick JD, McClanahan T, Kastelein RA, Cua DJ, IL-23 drives a pathogenic T cell population that induces autoimmune inflammation. J Exp Med 201, 233–240 (2005). [PubMed: 15657292]
4. Ivanov II, McKenzie BS, Zhou L, Tadokoro CE, Lepelley A, Lafaille JJ, Cua DJ, Littman DR, The orphan nuclear receptor RORgammat directs the differentiation program of proinflammatory IL-17+ T helper cells. Cell 126, 1121–1133 (2006). [PubMed: 16990136]
5. Wagner A, Wang C, Fessler J, DeTomaso D, Avila-Pacheco J, Kaminski J, Zaghouani S, Christian E, Thakore P, Schellhaass B, Akama-Garren E, Pierce K, Singh V, Ron-Harel N, Douglas VP, Bod L, Schnell A, Puleston D, Sobel RA, Haigis M, Pearce EL, Soleimani M, Clish C, Regev A, Kuchroo VK, Yosef N, Metabolic modeling of single Th17 cells reveals regulators of autoimmunity. Cell 184, 4168–4185 e4121 (2021). [PubMed: 34216539]
6. Annunziato F, Cosmi L, Santarlasci V, Maggi L, Liotta F, Mazzinghi B, Parente E, Fili L, Ferri S, Frosali F, Giudici F, Romagnani P, Parronchi P, Tonelli F, Maggi E, Romagnani S, Phenotypic and functional features of human Th17 cells. J Exp Med 204, 1849–1861 (2007). [PubMed: 17635957]
7. Kotake S, Udagawa N, Takahashi N, Matsuzaki K, Itoh K, Ishiyama S, Saito S, Inoue K, Kamatani N, Gillespie MT, Martin TJ, Suda T, IL-17 in synovial fluids from patients with rheumatoid arthritis is a potent stimulator of osteoclastogenesis. J Clin Invest 103, 1345–1352 (1999). [PubMed: 10225978]
8. Ziolkowska M, Koc A, Luszczykiewicz G, Ksiezopolska-Pietrzak K, Klimczak E, Chwalinska-Sadowska H, Maslinski W, High levels of IL-17 in rheumatoid arthritis patients: IL-15 triggers in vitro IL-17 production via cyclosporin A-sensitive mechanism. J Immunol 164, 2832–2838 (2000). [PubMed: 10679127]
9. Shahrara S, Huang Q, Mandelin AM 2nd, Pope RM, TH-17 cells in rheumatoid arthritis. Arthritis Res Ther 10, R93 (2008). [PubMed: 18710567]
10. Sarkar S, Cooney LA, Fox DA, The role of T helper type 17 cells in inflammatory arthritis. Clin Exp Immunol 159, 225–237 (2010). [PubMed: 19758374]
11. Hickman-Brecks CL, Racz JL, Meyer DM, LaBranche TP, Allen PM, Th17 cells can provide B cell help in autoantibody induced arthritis. J Autoimmun 36, 65–75 (2011). [PubMed: 21075597]
12. Genovese MC, Durez P, Richards HB, Supronik J, Dokoupilova E, Mazurov V, Aelion JA, Lee SH, Codding CE, Kellner H, Ikawa T, Hugot S, Mpofu S, Efficacy and safety of secukinumab in patients with rheumatoid arthritis: a phase II, dose-finding, double-blind, randomised, placebo controlled study. Ann Rheum Dis 72, 863–869 (2013). [PubMed: 22730366]

13. Genovese MC, Greenwald M, Cho CS, Berman A, Jin L, Cameron GS, Benichou O, Xie L, Braun D, Berclaz PY, Banerjee S, A phase II randomized study of subcutaneous ixekizumab, an anti-interleukin-17 monoclonal antibody, in rheumatoid arthritis patients who were naive to biologic agents or had an inadequate response to tumor necrosis factor inhibitors. Arthritis Rheumatol 66, 1693–1704 (2014). [PubMed: 24623718]

14. Tahir H, Deodhar A, Genovese M, Takeuchi T, Aelion J, Van den Bosch F, Haemmerle S, Richards HB, Secukinumab in Active Rheumatoid Arthritis after Anti-TNFalpha Therapy: A Randomized, Double-Blind Placebo-Controlled Phase 3 Study. Rheumatol Ther 4, 475–488 (2017). [PubMed: 29138986]

15. Zhang F, Wei K, Slowikowski K, Fonseka CY, Rao DA, Kelly S, Goodman SM, Tabechian D, Hughes LB, Salomon-Escoto K, Watts GFM, Jonsson AH, Rangel-Moreno J, Meednu N, Rozo C, Apruzzese W, Eisenhaure TM, Lieb DJ, Boyle DL, Mandelin AM 2nd, A. Accelerating Medicines Partnership Rheumatoid, C. Systemic Lupus Erythematosus, Boyce BF, DiCarlo E, Gravallese EM, Gregersen PK, Moreland L, Firestein GS, Hacohen N, Nusbaum C, Lederer JA, Perlman H, Pitzalis C, Filer A, Holers VM, Bykerk VP, Donlin LT, Anolik JH, Brenner MB, Raychaudhuri S, Defining inflammatory cell states in rheumatoid arthritis joint synovial tissues by integrating single-cell transcriptomics and mass cytometry. Nat Immunol 20, 928–942 (2019). [PubMed: 31061532]

16. Maggi L, Santarlasci V, Capone M, Rossi MC, Querci V, Mazzoni A, Cimaz R, De Palma R, Liotta F, Maggi E, Romagnani S, Cosmi L, Annunziato F, Distinctive features of classic and nonclassic (Th17 derived) human Th1 cells. Eur J Immunol 42, 3180–3188 (2012). [PubMed: 22965818]

17. Millier MJ, Fanning NC, Frampton C, Stamp LK, Hessian PA, Plasma interleukin-23 and circulating IL-17A(+)IFNgamma(+) ex-Th17 cells predict opposing outcomes of anti-TNF therapy in rheumatoid arthritis. Arthritis Res Ther 24, 57 (2022). [PubMed: 35219333]

18. Hirota K, Hashimoto M, Ito Y, Matsuura M, Ito H, Tanaka M, Watanabe H, Kondoh G, Tanaka A, Yasuda K, Kopf M, Potocnik AJ, Stockinger B, Sakaguchi N, Sakaguchi S, Autoimmune Th17 Cells Induced Synovial Stromal and Innate Lymphoid Cell Secretion of the Cytokine GM-CSF to Initiate and Augment Autoimmune Arthritis. Immunity 48, 1220–1232 e1225 (2018). [PubMed: 29802020]

19. Sakaguchi N, Takahashi T, Hata H, Nomura T, Tagami T, Yamazaki S, Sakihama T, Matsutani T, Negishi I, Nakatsuru S, Sakaguchi S, Altered thymic T-cell selection due to a mutation of the ZAP-70 gene causes autoimmune arthritis in mice. Nature 426, 454–460 (2003). [PubMed: 14647385]

20. Hirota K, Yoshitomi H, Hashimoto M, Maeda S, Teradaira S, Sugimoto N, Yamaguchi T, Nomura T, Ito H, Nakamura T, Sakaguchi N, Sakaguchi S, Preferential recruitment of CCR6-expressing Th17 cells to inflamed joints via CCL20 in rheumatoid arthritis and its animal model. J Exp Med 204, 2803–2812 (2007). [PubMed: 18025126]

21. Svensson MND, Zoccheddu M, Yang S, Nygaard G, Secchi C, Doody KM, Slowikowski K, Mizoguchi F, Humby F, Hands R, Santelli E, Sacchetti C, Wakabayashi K, Wu DJ, Barback C, Ai R, Wang W, Sims GP, Mydel P, Kasama T, Boyle DL, Galimi F, Vera D, Tremblay ML, Raychaudhuri S, Brenner MB, Firestein GS, Pitzalis C, Ekwall AH, Stanford SM, Bottini N, Synoviocyte-targeted therapy synergizes with TNF inhibition in arthritis reversal. Sci Adv 6, eaba4353 (2020). [PubMed: 32637608]

22. Hsieh WC, Svensson MN, Zoccheddu M, Tremblay ML, Sakaguchi S, Stanford SM, Bottini N, PTPN2 links colonic and joint inflammation in experimental autoimmune arthritis. JCI Insight 5, (2020).

23. Hashimoto M, Hirota K, Yoshitomi H, Maeda S, Teradaira S, Akizuki S, Prieto-Martin P, Nomura T, Sakaguchi N, Kohl J, Heyman B, Takahashi M, Fujita T, Mimori T, Sakaguchi S, Complement drives Th17 cell differentiation and triggers autoimmune arthritis. J Exp Med 207, 1135–1143 (2010). [PubMed: 20457757]

24. Ashouri JF, Hsu LY, Yu S, Rychkov D, Chen Y, Cheng DA, Sirota M, Hansen E, Lattanza L, Zikherman J, Weiss A, Reporters of TCR signaling identify arthritogenic T cells in murine and human autoimmune arthritis. Proc Natl Acad Sci U S A 116, 18517–18527 (2019). [PubMed: 31455730]

25. Matsuo T, Hashimoto M, Sakaguchi S, Sakaguchi N, Ito Y, Hikida M, Tsuruyama T, Sakai K, Yokoi H, Shirakashi M, Tanaka M, Ito H, Yoshifuji H, Ohmura K, Fujii T, Mimori T, Strain-Specific Manifestation of Lupus-like Systemic Autoimmunity Caused by Zap70 Mutation. J Immunol 202, 3161–3172 (2019). [PubMed: 31019063]
26. Tanaka A, Maeda S, Nomura T, Llamas-Covarrubias MA, Tanaka S, Jin L, Lim EL, Morikawa H, Kitagawa Y, Akizuki S, Ito Y, Fujimori C, Hirota K, Murase T, Hashimoto M, Higo J, Zamoyska R, Ueda R, Standley DM, Sakaguchi N, Sakaguchi S, Construction of a T cell receptor signaling range for spontaneous development of autoimmune disease. J Exp Med 220, (2023).
27. Bottini N, Firestein GS, Duality of fibroblast-like synoviocytes in RA: passive responders and imprinted aggressors. Nat Rev Rheumatol 9, 24–33 (2013). [PubMed: 23147896]
28. Hata H, Sakaguchi N, Yoshitomi H, Iwakura Y, Sekikawa K, Azuma Y, Kanai C, Moriizumi E, Nomura T, Nakamura T, Sakaguchi S, Distinct contribution of IL-6, TNF-alpha, IL-1, and IL-10 to T cell-mediated spontaneous autoimmune arthritis in mice. J Clin Invest 114, 582–588 (2004). [PubMed: 15314695]
29. Hirota K, Hashimoto M, Yoshitomi H, Tanaka S, Nomura T, Yamaguchi T, Iwakura Y, Sakaguchi N, Sakaguchi S, T cell self-reactivity forms a cytokine milieu for spontaneous development of IL-17+ Th cells that cause autoimmune arthritis. J Exp Med 204, 41–47 (2007). [PubMed: 17227914]
30. Svensson MN, Doody KM, Schmiedel BJ, Bhattacharyya S, Panwar B, Wiede F, Yang S, Santelli E, Wu DJ, Sacchetti C, Gujar R, Seumois G, Kiosses WB, Aubry I, Kim G, Mydel P, Sakaguchi S, Kronenberg M, Tiganis T, Tremblay ML, Ay F, Vijayanand P, Bottini N, Reduced expression of phosphatase PTPN2 promotes pathogenic conversion of Tregs in autoimmunity. J Clin Invest 129, 1193–1210 (2019). [PubMed: 30620725]
31. Hirota K, Duarte JH, Veldhoen M, Hornsby E, Li Y, Cua DJ, Ahlfors H, Wilhelm C, Tolaini M, Menzel U, Garefalaki A, Potocnik AJ, Stockinger B, Fate mapping of IL-17-producing T cells in inflammatory responses. Nat Immunol 12, 255–263 (2011). [PubMed: 21278737]
32. Madan R, Demircik F, Surianarayanan S, Allen JL, Divanovic S, Trompette A, Yogev N, Gu Y, Khodoun M, Hildeman D, Boespflug N, Fogolin MB, Grobe L, Greweling M, Finkelman FD, Cardin R, Mohrs M, Muller W, Waisman A, Roers A, Karp CL, Nonredundant roles for B cell-derived IL-10 in immune counter-regulation. J Immunol 183, 2312–2320 (2009). [PubMed: 19620304]
33. Reinhardt RL, Liang HE, Locksley RM, Cytokine-secreting follicular T cells shape the antibody repertoire. Nat Immunol 10, 385–393 (2009). [PubMed: 19252490]
34. Madisen L, Zwingman TA, Sunkin SM, Oh SW, Zariwala HA, Gu H, Ng LL, Palmiter RD, Hawrylycz MJ, Jones AR, Lein ES, Zeng H, A robust and high-throughput Cre reporting and characterization system for the whole mouse brain. Nat Neurosci 13, 133–140 (2010). [PubMed: 20023653]
35. McHugh J, The many faces of TNF in arthritis. Nat Rev Rheumatol 16, 603 (2020).
36. Choy EH, De Benedetti F, Takeuchi T, Hashizume M, John MR, Kishimoto T, Translating IL-6 biology into effective treatments. Nat Rev Rheumatol 16, 335–345 (2020). [PubMed: 32327746]
37. Gagliani N, Amezcua Vesely MC, Iseppon A, Brockmann L, Xu H, Palm NW, de Zoete MR, Licona-Limon P, Paiva RS, Ching T, Weaver C, Zi X, Pan X, Fan R, Garmire LX, Cotton MJ, Drier Y, Bernstein B, Geginat J, Stockinger B, Esplugues E, Huber S, Flavell RA, Th17 cells transdifferentiate into regulatory T cells during resolution of inflammation. Nature 523, 221–225 (2015). [PubMed: 25924064]
38. Manzo A, Paoletti S, Carulli M, Blades MC, Barone F, Yanni G, Fitzgerald O, Bresnihan B, Caporali R, Montecucco C, Uguccioni M, Pitzalis C, Systematic microanatomical analysis of CXCL13 and CCL21 in situ production and progressive lymphoid organization in rheumatoid synovitis. Eur J Immunol 35, 1347–1359 (2005). [PubMed: 15832291]
39. Amezcua Vesely MC, Pallis P, Bielecki P, Low JS, Zhao J, Harman CCD, Kroehling L, Jackson R, Bailis W, Licona-Limon P, Xu H, Iijima N, Pillai PS, Kaplan DH, Weaver CT, Kluger Y, Kowalczyk MS, Iwasaki A, Pereira JP, Esplugues E, Gagliani N, Flavell RA, Effector T(H)17 Cells Give Rise to Long-Lived T(RM) Cells that Are Essential for an Immediate Response against Bacterial Infection. Cell 178, 1176–1188 e1115 (2019). [PubMed: 31442406]

40. Butterfield K, Fathman CG, Budd RC, A subset of memory CD4+ helper T lymphocytes identified by expression of Pgp-1. J Exp Med 169, 1461–1466 (1989). [PubMed: 2564418]
41. von Werdt D, Gungor B, Barreto de Albuquerque J, Gruber T, Zysset D, Kwong Chung CKC, Correa-Ferreira A, Berchtold R, Page N, Schenk M, Kehrl JH, Merkler D, Imhof BA, Stein JV, Abe J, Turchinovich G, Finke D, Hayday AC, Corazza N, Mueller C, Regulator of G-protein signaling 1 critically supports CD8(+) T(RM) cell-mediated intestinal immunity. Front Immunol 14, 1085895 (2023). [PubMed: 37153600]
42. Liu SK, Fang N, Koretzky GA, McGlade CJ, The hematopoietic-specific adaptor protein gads functions in T-cell signaling via interactions with the SLP-76 and LAT adaptors. Curr Biol 9, 67–75 (1999). [PubMed: 10021361]
43. Filen JJ, Filen S, Moulder R, Tuomela S, Ahlfors H, West A, Kouvonen P, Kantola S, Bjorkman M, Katajamaa M, Rasool O, Nyman TA, Lahesmaa R, Quantitative proteomics reveals GIMAP family proteins 1 and 4 to be differentially regulated during human T helper cell differentiation. Mol Cell Proteomics 8, 32–44 (2009). [PubMed: 18701445]
44. Trevino AE, Muller F, Andersen J, Sundaram L, Kathiria A, Shcherbina A, Farh K, Chang HY, Pasca AM, Kundaje A, Pasca SP, Greenleaf WJ, Chromatin and gene-regulatory dynamics of the developing human cerebral cortex at single-cell resolution. Cell 184, 5053–5069 e5023 (2021). [PubMed: 34390642]
45. Seumois G, Ramirez-Suastegui C, Schmiedel BJ, Liang S, Peters B, Sette A, Vijayanand P, Single-cell transcriptomic analysis of allergen-specific T cells in allergy and asthma. Sci Immunol 5, (2020).
46. Best JA, Blair DA, Knell J, Yang E, Mayya V, Doedens A, Dustin ML, Goldrath AW, Immunological Genome Project C, Transcriptional insights into the CD8(+) T cell response to infection and memory T cell formation. Nat Immunol 14, 404–412 (2013). [PubMed: 23396170]
47. Ashouri J, McCarthy E, Yu S, Perlmutter N, Lin C, DeRisi J, Ye CJ, Weiss A, Naïve arthritogenic SKG T cells have a defect in anergy and a repertoire pruned by superantigen. bioRxiv, 2022.2001.2013.476250 (2022).
48. Wu J, Feng Z, Chen L, Li Y, Bian H, Geng J, Zheng ZH, Fu X, Pei Z, Qin Y, Yang L, Zhao Y, Wang K, Chen R, He Q, Nan G, Jiang X, Chen ZN, Zhu P, TNF antagonist sensitizes synovial fibroblasts to ferroptotic cell death in collagen-induced arthritis mouse models. Nat Commun 13, 676 (2022). [PubMed: 35115492]
49. Zhang F, Jonsson AH, Nathan A, Millard N, Curtis M, Xiao Q, Gutierrez-Arcelus M, Apruzzese W, Watts GFM, Weisenfeld D, Nayar S, Rangel-Moreno J, Meednu N, Marks KE, Mantel I, Kang JB, Rumker L, Mears J, Slowikowski K, Weinand K, Orange DE, Geraldino-Pardilla L, Deane KD, Tabechian D, Ceponis A, Firestein GS, Maybury M, Sahbudin I, Ben-Artzi A, Mandelin AM 2nd, Nerviani A, Lewis MJ, Rivellese F, Pitzalis C, Hughes LB, Horowitz D, DiCarlo E, Gravallese EM, Boyce BF, Accelerating Medicines Partnership RASLEN, Moreland LW, Goodman SM, Perlman H, Holers VM, Liao KP, Filer A, Bykerk VP, Wei K, Rao DA, Donlin LT, Anolik JH, Brenner MB, Raychaudhuri S, Deconstruction of rheumatoid arthritis synovium defines inflammatory subtypes. Nature 623, 616–624 (2023). [PubMed: 37938773]
50. Rao DA, Gurish MF, Marshall JL, Slowikowski K, Fonseka CY, Liu Y, Donlin LT, Henderson LA, Wei K, Mizoguchi F, Teslovich NC, Weinblatt ME, Massarotti EM, Coblyn JS, Helfgott SM, Lee YC, Todd DJ, Bykerk VP, Goodman SM, Pernis AB, Ivashkiv LB, Karlson EW, Nigrovic PA, Filer A, Buckley CD, Lederer JA, Raychaudhuri S, Brenner MB, Pathologically expanded peripheral T helper cell subset drives B cells in rheumatoid arthritis. Nature 542, 110–114 (2017). [PubMed: 28150777]
51. Ichiyama K, Long J, Kobayashi Y, Horita Y, Kinoshita T, Nakamura Y, Kominami C, Georgopoulos K, Sakaguchi S, Transcription factor Ikzf1 associates with Foxp3 to repress gene expression in Treg cells and limit autoimmunity and anti-tumor immunity. Immunity 57, 2043–2060 e2010 (2024). [PubMed: 39111316]
52. Leung S, Qureshi SA, Kerr IM, Darnell JE Jr., Stark GR, Role of STAT2 in the alpha interferon signaling pathway. Mol Cell Biol 15, 1312–1317 (1995). [PubMed: 7532278]
53. Shamovsky I, Nudler E, New insights into the mechanism of heat shock response activation. Cell Mol Life Sci 65, 855–861 (2008). [PubMed: 18239856]

54. Pham D, Silberger DJ, Nguyen KN, Gao M, Weaver CT, Hatton RD, Batf stabilizes Th17 cell development via impaired Stat5 recruitment of Ets1-Runx1 complexes. EMBO J 42, e109803 (2023). [PubMed: 36917143]
55. Yang L, Anderson DE, Baecher-Allan C, Hastings WD, Bettelli E, Oukka M, Kuchroo VK, Hafler DA, IL-21 and TGF-beta are required for differentiation of human T(H)17 cells. Nature 454, 350–352 (2008). [PubMed: 18469800]
56. Park YJ, Yoo SA, Kim M, Kim WU, The Role of Calcium-Calcineurin-NFAT Signaling Pathway in Health and Autoimmune Diseases. Front Immunol 11, 195 (2020). [PubMed: 32210952]
57. Hiwa R, Brooks JF, Mueller JL, Nielsen HV, Zikherman J, NR4A nuclear receptors in T and B lymphocytes: Gatekeepers of immune tolerance(). Immunol Rev 307, 116–133 (2022). [PubMed: 35174510]
58. Li C, Virgilio MC, Collins KL, Welch JD, Multi-omic single-cell velocity models epigenome-transcriptome interactions and improves cell fate prediction. Nat Biotechnol 41, 387–398 (2023). [PubMed: 36229609]
59. Komatsu N, Okamoto K, Sawa S, Nakashima T, Oh-hora M, Kodama T, Tanaka S, Bluestone JA, Takayanagi H, Pathogenic conversion of Foxp3+ T cells into TH17 cells in autoimmune arthritis. Nat Med 20, 62–68 (2014). [PubMed: 24362934]
60. Tanevski J, Flores ROR, Gabor A, Schapiro D, Saez-Rodriguez J, Explainable multiview framework for dissecting spatial relationships from highly multiplexed data. Genome Biol 23, 97 (2022). [PubMed: 35422018]
61. Janesick A, Shelansky R, Gottscho AD, Wagner F, Williams SR, Rouault M, Beliakoff G, Morrison CA, Oliveira MF, Sicherman JT, Kohlway A, Abousoud J, Drennon TY, Mohabbat SH, x Development T, Taylor SEB, High resolution mapping of the tumor microenvironment using integrated single-cell, spatial and in situ analysis. Nat Commun 14, 8353 (2023). [PubMed: 38114474]
62. Schwachula A, Riemann D, Kehlen A, Langner J, Characterization of the immunophenotype and functional properties of fibroblast-like synoviocytes in comparison to skin fibroblasts and umbilical vein endothelial cells. Immunobiology 190, 67–92 (1994). [PubMed: 8082888]
63. Harada S, Yamamura M, Okamoto H, Morita Y, Kawashima M, Aita T, Makino H, Production of interleukin-7 and interleukin-15 by fibroblast-like synoviocytes from patients with rheumatoid arthritis. Arthritis Rheum 42, 1508–1516 (1999). [PubMed: 10403280]
64. Brennan FM, Hayes AL, Ciesielski CJ, Green P, Foxwell BM, Feldmann M, Evidence that rheumatoid arthritis synovial T cells are similar to cytokine-activated T cells: involvement of phosphatidylinositol 3-kinase and nuclear factor kappaB pathways in tumor necrosis factor alpha production in rheumatoid arthritis. Arthritis Rheum 46, 31–41 (2002). [PubMed: 11822409]
65. Lai WQ, Irwan AW, Goh HH, Howe HS, Yu DT, Valle-Onate R, McInnes IB, Melendez AJ, Leung BP, Anti-inflammatory effects of sphingosine kinase modulation in inflammatory arthritis. J Immunol 181, 8010–8017 (2008). [PubMed: 19017993]
66. Zhao C, Moreno-Nieves U, Di Battista JA, Fernandes MJ, Touaibia M, Bourgoin SG, Chemical Hypoxia Brings to Light Altered Autocrine Sphingosine-1-Phosphate Signalling in Rheumatoid Arthritis Synovial Fibroblasts. Mediators Inflamm 2015, 436525 (2015). [PubMed: 26556954]
67. Cencetti F, Bernacchioni C, Tonelli F, Roberts E, Donati C, Bruni P, TGFbeta1 evokes myoblast apoptotic response via a novel signaling pathway involving S1P4 transactivation upstream of Rho-kinase-2 activation. FASEB J 27, 4532–4546 (2013). [PubMed: 23913862]
68. Schwab SR, Cyster JG, Finding a way out: lymphocyte egress from lymphoid organs. Nat Immunol 8, 1295–1301 (2007). [PubMed: 18026082]
69. Bravo GA, Cedeno RR, Casadevall MP, Ramio-Torrenta L, Sphingosine-1-Phosphate (S1P) and S1P Signaling Pathway Modulators, from Current Insights to Future Perspectives. Cells 11, (2022).
70. Tsunemi S, Iwasaki T, Kitano S, Imado T, Miyazawa K, Sano H, Effects of the novel immunosuppressant FTY720 in a murine rheumatoid arthritis model. Clin Immunol 136, 197–204 (2010). [PubMed: 20421177]
71. Naor D, Nedvetzki S, CD44 in rheumatoid arthritis. Arthritis Res Ther 5, 105–115 (2003). [PubMed: 12723975]

72. Yoo SA, Leng L, Kim BJ, Du X, Tilstam PV, Kim KH, Kong JS, Yoon HJ, Liu A, Wang T, Song Y, Sauler M, Bernhagen J, Ritchlin CT, Lee P, Cho CS, Kim WU, Bucala R, MIF allele-dependent regulation of the MIF coreceptor CD44 and role in rheumatoid arthritis. Proc Natl Acad Sci U S A 113, E7917–E7926 (2016). [PubMed: 27872288]
73. Yoshioka Y, Kozawa E, Urakawa H, Arai E, Futamura N, Zhuo L, Kimata K, Ishiguro N, Nishida Y, Suppression of hyaluronan synthesis alleviates inflammatory responses in murine arthritis and in human rheumatoid synovial fibroblasts. Arthritis Rheum 65, 1160–1170 (2013). [PubMed: 23335273]
74. Brennan FR, Mikecz K, Glant TT, Jobanputra P, Pinder S, Bavington C, Morrison P, Nuki G, CD44 expression by leucocytes in rheumatoid arthritis and modulation by specific antibody: implications for lymphocyte adhesion to endothelial cells and synoviocytes in vitro. Scand J Immunol 45, 213–220 (1997). [PubMed: 9042434]
75. Baaten BJ, Tinoco R, Chen AT, Bradley LM, Regulation of Antigen-Experienced T Cells: Lessons from the Quintessential Memory Marker CD44. Front Immunol 3, 23 (2012). [PubMed: 22566907]
76. Liao JJ, Huang MC, Goetzl EJ, Cutting edge: Alternative signaling of Th17 cell development by sphingosine 1-phosphate. J Immunol 178, 5425–5428 (2007). [PubMed: 17442922]
77. Baker DA, Obeid LM, Gilkeson GS, Impact of sphingosine kinase on inflammatory pathways in fibroblast-like synoviocytes. Inflamm Allergy Drug Targets 10, 464–471 (2011). [PubMed: 21864273]
78. Zhu C, Wen S, Li J, Meng H, Zhang J, Zhao K, Wang L, Zhang Y, FTY720 Inhibits the Development of Collagen-Induced Arthritis in Mice by Suppressing the Recruitment of CD4(+) T Lymphocytes. Drug Des Devel Ther 15, 1981–1992 (2021).
79. Jin J, Ji M, Fu R, Wang M, Xue N, Xiao Q, Hu J, Wang X, Lai F, Yin D, Chen X, Sphingosine-1-Phosphate Receptor Subtype 1 (S1P1) Modulator IMMH001 Regulates Adjuvant- and Collagen-Induced Arthritis. Front Pharmacol 10, 1085 (2019). [PubMed: 31607926]
80. Lesley J, Hyman R, Kincade PW, CD44 and its interaction with extracellular matrix. Adv Immunol 54, 271–335 (1993). [PubMed: 8379464]
81. Siegelman MH, DeGrendele HC, Estess P, Activation and interaction of CD44 and hyaluronan in immunological systems. J Leukoc Biol 66, 315–321 (1999). [PubMed: 10449175]
82. Nagy N, Kuipers HF, Marshall PL, Wang E, Kaber G, Bollyky PL, Hyaluronan in immune dysregulation and autoimmune diseases. Matrix Biol 78–79, 292–313 (2019).
83. Borjini N, Lun Y, Jang GF, Crabb J, Chen Y, Crabb J, Fox DA, Ivanov AI, Lin F, CD6 triggers actomyosin cytoskeleton remodeling after binding to its receptor complex. J Leukoc Biol 115, 450–462 (2024). [PubMed: 37820034]
84. Cubuk C, Lau R, Cutillas P, Rajeeve V, John CR, Surace AEA, Hands R, Fossati-Jimack L, Lewis MJ, Pitzalis C, Phosphoproteomic profiling of early rheumatoid arthritis synovium reveals active signalling pathways and differentiates inflammatory pathotypes. Arthritis Res Ther 26, 120 (2024). [PubMed: 38867295]
85. El Shikh MEM, El Sayed R, Aly NAR, Prediletto E, Hands R, Fossati-Jimack L, Bombardieri M, Lewis MJ, Pitzalis C, Follicular dendritic cell differentiation is associated with distinct synovial pathotype signatures in rheumatoid arthritis. Front Med (Lausanne) 9, 1013660 (2022). [PubMed: 36465908]
86. Cooles FAH, Anderson AE, Lendrem DW, Norris J, Pratt AG, Hilkens CMU, Isaacs JD, The interferon gene signature is increased in patients with early treatment-naive rheumatoid arthritis and predicts a poorer response to initial therapy. J Allergy Clin Immunol 141, 445–448 e444 (2018). [PubMed: 28987811]
87. Chang MH, Levescot A, Nelson-Maney N, Blaustein RB, Winden KD, Morris A, Wactor A, Balu S, Grieshaber-Bouyer R, Wei K, Henderson LA, Iwakura Y, Clark RA, Rao DA, Fuhlbrigge RC, Nigrovic PA, Arthritis flares mediated by tissue-resident memory T cells in the joint. Cell Rep 37, 109902 (2021). [PubMed: 34706228]
88. Jonsson AH, Zhang F, Dunlap G, Gomez-Rivas E, Watts GFM, Faust HJ, Rupani KV, Mears JR, Meednu N, Wang R, Keras G, Coblyn JS, Massarotti EM, Todd DJ, Anolik JH, McDavid A, Accelerating Medicines Partnership RASLEN, Wei K, Rao DA, Raychaudhuri S, Brenner MB,

Granzyme K(+) CD8 T cells form a core population in inflamed human tissue. Sci Transl Med 14, eabo0686 (2022). [PubMed: 35704599]

89. Benham H, Rehaume LM, Hasnain SZ, Velasco J, Baillet AC, Ruutu M, Kikly K, Wang R, Tseng HW, Thomas GP, Brown MA, Strutton G, McGuckin MA, Thomas R, Interleukin-23 mediates the intestinal response to microbial beta-1,3-glucan and the development of spondyloarthritis pathology in SKG mice. Arthritis Rheumatol 66, 1755–1767 (2014). [PubMed: 24664521]
90. Ruutu M, Thomas G, Steck R, Degli-Esposti MA, Zinkernagel MS, Alexander K, Velasco J, Strutton G, Tran A, Benham H, Rehaume L, Wilson RJ, Kikly K, Davies J, Pettit AR, Brown MA, McGuckin MA, Thomas R, beta-glucan triggers spondylarthritis and Crohn's disease-like ileitis in SKG mice. Arthritis Rheum 64, 2211–2222 (2012). [PubMed: 22328069]
91. James EA, Holers VM, Iyer R, Prideaux EB, Rao NL, Rims C, Muir VS, Posso SE, Bloom MS, Zia A, Elliott SE, Adamska JZ, Ai R, Brewer RC, Seifert JA, Moss L, Barzideh S, Demoruelle MK, Striebich CC, Okamoto Y, Sainbayar E, Crook AA, Peterson RA, Vanderlinden LA, Wang W, Boyle DL, Robinson WH, Buckner JH, Firestein GS, Deane KD, Multifaceted immune dysregulation characterizes individuals at-risk for rheumatoid arthritis. Nat Commun 14, 7637 (2023). [PubMed: 37993439]
92. Inamo J, Keegan J, Griffith A, Ghosh T, Horisberger A, Howard K, Pulford JF, Murzin E, Hancock B, Dominguez ST, Gurra MG, Gurajala S, Jonsson AH, Seifert JA, Feser ML, Norris JM, Cao Y, Apruzzese W, Bridges SL, Bykerk VP, Goodman S, Donlin LT, Firestein GS, Bathon JM, Hughes LB, Filer A, Pitzalis C, Anolik JH, Moreland L, Hacohen N, Guthridge JM, James JA, Cuda CM, Perlman H, Brenner MB, Raychaudhuri S, Sparks JA, Accelerating Medicines Partnership RASLEN, Holers VM, Deane KD, Lederer J, Rao DA, Zhang F, Deep immunophenotyping reveals circulating activated lymphocytes in individuals at risk for rheumatoid arthritis. J Clin Invest 135, (2025).
93. Scher JU, Ubeda C, Equinda M, Khanin R, Buischi Y, Viale A, Lipuma L, Attur M, Pillinger MH, Weissmann G, Littman DR, Pamer EG, Bretz WA, Abramson SB, Periodontal disease and the oral microbiota in new-onset rheumatoid arthritis. Arthritis Rheum 64, 3083–3094 (2012). [PubMed: 22576262]
94. Scher JU, Sczesnak A, Longman RS, Segata N, Ubeda C, Bielski C, Rostron T, Cerundolo V, Pamer EG, Abramson SB, Huttenhower C, Littman DR, Expansion of intestinal Prevotella copri correlates with enhanced susceptibility to arthritis. Elife 2, e01202 (2013). [PubMed: 24192039]
95. Hayer S, Vervoordeldonk MJ, Denis MC, Armaka M, Hoffmann M, Backlund J, Nandakumar KS, Niederreiter B, Geka C, Fischer A, Woodworth N, Bluml S, Kollias G, Holmdahl R, Apparailly F, Koenders MI, 'SMASH' recommendations for standardised microscopic arthritis scoring of histological sections from inflammatory arthritis animal models. Ann Rheum Dis 80, 714–726 (2021). [PubMed: 33602797]
96. Hao Z, Rajewsky K, Homeostasis of peripheral B cells in the absence of B cell influx from the bone marrow. J Exp Med 194, 1151–1164 (2001). [PubMed: 11602643]
97. Price AE, Reinhardt RL, Liang HE, Locksley RM, Marking and quantifying IL-17A-producing cells in vivo. PLoS One 7, e39750 (2012). [PubMed: 22768117]
98. Bankhead P, Loughrey MB, Fernandez JA, Dombrowski Y, McArt DG, Dunne PD, McQuaid S, Gray RT, Murray LJ, Coleman HG, James JA, Salto-Tellez M, Hamilton PW, QuPath: Open source software for digital pathology image analysis. Sci Rep 7, 16878 (2017). [PubMed: 29203879]
99. McBride DA, Kerr MD, Johnson WT, Nguyen A, Zoccheddu M, Yao M, Prideaux EB, Dorn NC, Wang W, Svensson MND, Bottini N, Shah NJ, Immunomodulatory Microparticles Epigenetically Modulate T Cells and Systemically Ameliorate Autoimmune Arthritis. Adv Sci (Weinh), e2202720 (2023). [PubMed: 36890657]
100. Chen S, Zhou Y, Chen Y, Gu J, fastp: an ultra-fast all-in-one FASTQ preprocessor. Bioinformatics 34, i884–i890 (2018). [PubMed: 30423086]
101. Dobin A, Davis CA, Schlesinger F, Drenkow J, Zaleski C, Jha S, Batut P, Chaisson M, Gingeras TR, STAR: ultrafast universal RNA-seq aligner. Bioinformatics 29, 15–21 (2013). [PubMed: 23104886]
102. Love MI, Huber W, Anders S, Moderated estimation of fold change and dispersion for RNA-seq data with DESeq2. Genome Biol 15, 550 (2014). [PubMed: 25516281]

103. Zhou Y, Zhou B, Pache L, Chang M, Khodabakhshi AH, Tanaseichuk O, Benner C, Chanda SK, Metascape provides a biologist-oriented resource for the analysis of systems-level datasets. Nat Commun 10, 1523 (2019). [PubMed: 30944313]
104. Shannon P, Markiel A, Ozier O, Baliga NS, Wang JT, Ramage D, Amin N, Schwikowski B, Ideker T, Cytoscape: a software environment for integrated models of biomolecular interaction networks. Genome Res 13, 2498–2504 (2003). [PubMed: 14597658]
105. Stuart T, Srivastava A, Madad S, Lareau CA, Satija R, Single-cell chromatin state analysis with Signac. Nat Methods 18, 1333–1341 (2021). [PubMed: 34725479]
106. Zhang Y, Liu T, Meyer CA, Eeckhoute J, Johnson DS, Bernstein BE, Nusbaum C, Myers RM, Brown M, Li W, Liu XS, Model-based analysis of ChIP-Seq (MACS). Genome Biol 9, R137 (2008). [PubMed: 18798982]
107. Korsunsky I, Millard N, Fan J, Slowikowski K, Zhang F, Wei K, Baglaenko Y, Brenner M, Loh PR, Raychaudhuri S, Fast, sensitive and accurate integration of single-cell data with Harmony. Nat Methods 16, 1289–1296 (2019). [PubMed: 31740819]
108. Arnett FC, Edworthy SM, Bloch DA, McShane DJ, Fries JF, Cooper NS, Healey LA, Kaplan SR, Liang MH, Luthra HS, et al. , The American Rheumatism Association 1987 revised criteria for the classification of rheumatoid arthritis. Arthritis Rheum 31, 315–324 (1988). [PubMed: 3358796]
109. Aletaha D, Neogi T, Silman AJ, Funovits J, Felson DT, Bingham CO 3rd, Birnbaum NS, Burmester GR, Bykerk VP, Cohen MD, Combe B, Costenbader KH, Dougados M, Emery P, Ferraccioli G, Hazes JM, Hobbs K, Huizinga TW, Kavanaugh A, Kay J, Kvien TK, Laing T, Mease P, Menard HA, Moreland LW, Naden RL, Pincus T, Smolen JS, Stanislawska-Biernat E, Symmons D, Tak PP, Upchurch KS, Vencovsky J, Wolfe F, Hawker G, 2010 Rheumatoid arthritis classification criteria: an American College of Rheumatology/European League Against Rheumatism collaborative initiative. Arthritis Rheum 62, 2569–2581 (2010). [PubMed: 20872595]
110. Kelly S, Humby F, Filer A, Ng N, Di Cicco M, Hands RE, Rocher V, Bombardieri M, D'Agostino MA, McInnes IB, Buckley CD, Taylor PC, Pitzalis C, Ultrasound-guided synovial biopsy: a safe, well-tolerated and reliable technique for obtaining high-quality synovial tissue from both large and small joints in early arthritis patients. Ann Rheum Dis 74, 611–617 (2015). [PubMed: 24336336]
111. Mandelin AM 2nd, Homan PJ, Shaffer AM, Cuda CM, Dominguez ST, Bacalao E, Carns M, Hinchcliff M, Lee J, Aren K, Thakrar A, Montgomery AB, Louis Bridges S Jr., Bathon JM, Atkinson JP, Fox DA, Matteson EL, Buckley CD, Pitzalis C, Parks D, Hughes LB, Geraldino-Pardilla L, Ike R, Phillips K, Wright K, Filer A, Kelly S, Ruderman EM, Morgan V, Abdala-Valencia H, Misharin AV, Budinger GS, Bartom ET, Pope RM, Perlman H, Winter DR, Transcriptional Profiling of Synovial Macrophages using Minimally Invasive Ultrasound-Guided Synovial Biopsies in Rheumatoid Arthritis. Arthritis & rheumatology, (2018).
112. Filkova M, Cope A, Mant T, Galloway J, Is there a role of synovial biopsy in drug development? BMC Musculoskelet Disord 17, 172 (2016). [PubMed: 27094362]
113. Gerlag DM, Tak PP, How to perform and analyse synovial biopsies. Best Pract Res Clin Rheumatol 27, 195–207 (2013). [PubMed: 23731931]
114. Humby F, Kelly S, Bugatti S, Manzo A, Filer A, Mahto A, Fonseca JE, Lauwerys B, D'Agostino MA, Naredo E, Lories R, Montecucco C, Tak PP, Fitzgerald O, Smith MD, Veale DJ, Choy EH, Strand V, Pitzalis C, Evaluation of Minimally Invasive, Ultrasound-guided Synovial Biopsy Techniques by the OMERACT Filter--Determining Validation Requirements. J Rheumatol 43, 208–213 (2016). [PubMed: 26034155]
115. Humby F, Kelly S, Hands R, Rocher V, DiCicco M, Ng N, Zou L, Bugatti S, Manzo A, Caporali R, Montecucco C, Bombardieri M, Pitzalis C, Use of ultrasound-guided small joint biopsy to evaluate the histopathologic response to rheumatoid arthritis therapy: recommendations for application to clinical trials. Arthritis Rheumatol 67, 2601–2610 (2015). [PubMed: 26097225]
116. Koski JM, Helle M, Ultrasound guided synovial biopsy using portal and forceps. Ann Rheum Dis 64, 926–929 (2005). [PubMed: 15550535]
117. Lazarou I, D'Agostino MA, Naredo E, Humby F, Filer A, Kelly SG, Ultrasound-guided synovial biopsy: a systematic review according to the OMERACT filter and recommendations for minimal

reporting standards in clinical studies. Rheumatology (Oxford) 54, 1867–1875 (2015). [PubMed: 26022188]

118. Ramirez J, Celis R, Usategui A, Ruiz-Esquide V, Fare R, Cuervo A, Sanmarti R, Pablos JL, Canete JD, Immunopathologic characterization of ultrasound-defined synovitis in rheumatoid arthritis patients in clinical remission. Arthritis Res Ther 18, 74 (2015).
119. Scire CA, Epis O, Codullo V, Humby F, Morbini P, Manzo A, Caporali R, Pitzalis C, Montecucco C, Immunohistological assessment of the synovial tissue in small joints in rheumatoid arthritis: validation of a minimally invasive ultrasound-guided synovial biopsy procedure. Arthritis Res Ther 9, R101 (2007). [PubMed: 17903238]
120. Sitt JC, Griffith JF, Wong P, Ultrasound-guided synovial biopsy. Br J Radiol 89, 20150363 (2016). [PubMed: 26581578]
121. van Vugt RM, van Dalen A, Bijlsma JW, Ultrasound guided synovial biopsy of the wrist. Scand J Rheumatol 26, 212–214 (1997). [PubMed: 9225877]
122. Filer A, de Pablo P, Allen G, Nightingale P, Jordan A, Jobanputra P, Bowman S, Buckley CD, Raza K, Utility of ultrasound joint counts in the prediction of rheumatoid arthritis in patients with very early synovitis. Ann Rheum Dis 70, 500–507 (2011). [PubMed: 21115552]
123. Filkova M, Aradi B, Senolt L, Ospelt C, Vettori S, Mann H, Filer A, Raza K, Buckley CD, Snow M, Vencovsky J, Pavelka K, Michel BA, Gay RE, Gay S, Jungel A, Association of circulating miR-223 and miR-16 with disease activity in patients with early rheumatoid arthritis. Ann Rheum Dis, (2013).
124. Pitzalis C, Kelly S, Humby F, New learnings on the pathophysiology of RA from synovial biopsies. Curr Opin Rheumatol 25, 334–344 (2013). [PubMed: 23492740]
125. Yeo L, Toellner KM, Salmon M, Filer A, Buckley CD, Raza K, Scheel-Toellner D, Cytokine mRNA profiling identifies B cells as a major source of RANKL in rheumatoid arthritis. Ann Rheum Dis 70, 2022–2028 (2011). [PubMed: 21742639]
126. Kraan MC, Reece RJ, Smeets TJ, Veale DJ, Emery P, Tak PP, Comparison of synovial tissues from the knee joints and the small joints of rheumatoid arthritis patients: Implications for pathogenesis and evaluation of treatment. Arthritis Rheum 46, 2034–2038 (2002). [PubMed: 12209505]
127. Donlin LT, Rao DA, Wei K, Slowikowski K, McGeachy MJ, Turner JD, Meednu N, Mizoguchi F, Gutierrez-Arcelus M, Lieb DJ, Keegan J, Muskat K, Hillman J, Rozo C, Ricker E, Eisenhaure TM, Li S, Browne EP, Chicoine A, Sutherby D, Noma A, Accelerating Medicines Partnership RASLEN, Nusbaum C, Kelly S, Pernis AB, Ivashkiv LB, Goodman SM, Robinson WH, Utz PJ, Lederer JA, Gravallese EM, Boyce BF, Hacohen N, Pitzalis C, Gregersen PK, Firestein GS, Raychaudhuri S, Moreland LW, Holers VM, Bykerk VP, Filer A, Boyle DL, Brenner MB, Anolik JH, Methods for high-dimensonal analysis of cells dissociated from cyropreserved synovial tissue. Arthritis Res Ther 20, 139 (2018). [PubMed: 29996944]
128. La Manno G, Soldatov R, Zeisel A, Braun E, Hochgerner H, Petukhov V, Lidschreiber K, Kastriti ME, Lonnerberg P, Furlan A, Fan J, Borm LE, Liu Z, van Bruggen D, Guo J, He X, Barker R, Sundstrom E, Castelo-Branco G, Cramer P, Adameyko I, Linnarsson S, Kharchenko PV, RNA velocity of single cells. Nature 560, 494–498 (2018). [PubMed: 30089906]
129. Bergen V, Lange M, Peidli S, Wolf FA, Theis FJ, Generalizing RNA velocity to transient cell states through dynamical modeling. Nat Biotechnol 38, 1408–1414 (2020). [PubMed: 32747759]
130. Bravo Gonzalez-Blas C, De Winter S, Hulselmans G, Hecker N, Matetovici I, Christiaens V, Poovathingal S, Wouters J, Aibar S, Aerts S, SCENIC+: single-cell multiomic inference of enhancers and gene regulatory networks. Nat Methods, (2023).
131. Hao Y, Hao S, Andersen-Nissen E, Mauck WM 3rd, Zheng S, Butler A, Lee MJ, Wilk AJ, Darby C, Zager M, Hoffman P, Stoeckius M, Papalexi E, Mimitou EP, Jain J, Srivastava A, Stuart T, Fleming LM, Yeung B, Rogers AJ, McElrath JM, Blish CA, Gottardo R, Smibert P, Satija R, Integrated analysis of multimodal single-cell data. Cell 184, 3573–3587 e3529 (2021). [PubMed: 34062119]
132. Hafemeister C, Satija R, Normalization and variance stabilization of single-cell RNA-seq data using regularized negative binomial regression. Genome Biol 20, 296 (2019). [PubMed: 31870423]

133. Ravi VM, Will P, Kueckelhaus J, Sun N, Joseph K, Salie H, Vollmer L, Kuliesiute U, von Ehr J, Benotmane JK, Neidert N, Follo M, Scherer F, Goeldner JM, Behringer SP, Franco P, Khiat M, Zhang J, Hofmann UG, Fung C, Ricklefs FL, Lamszus K, Boerries M, Ku M, Beck J, Sankowski R, Schwabenland M, Prinz M, Schuller U, Killmer S, Bengsch B, Walch AK, Delev D, Schnell O, Heiland DH, Spatially resolved multi-omics deciphers bidirectional tumor-host interdependence in glioblastoma. Cancer Cell 40, 639–655 e613 (2022). [PubMed: 35700707]

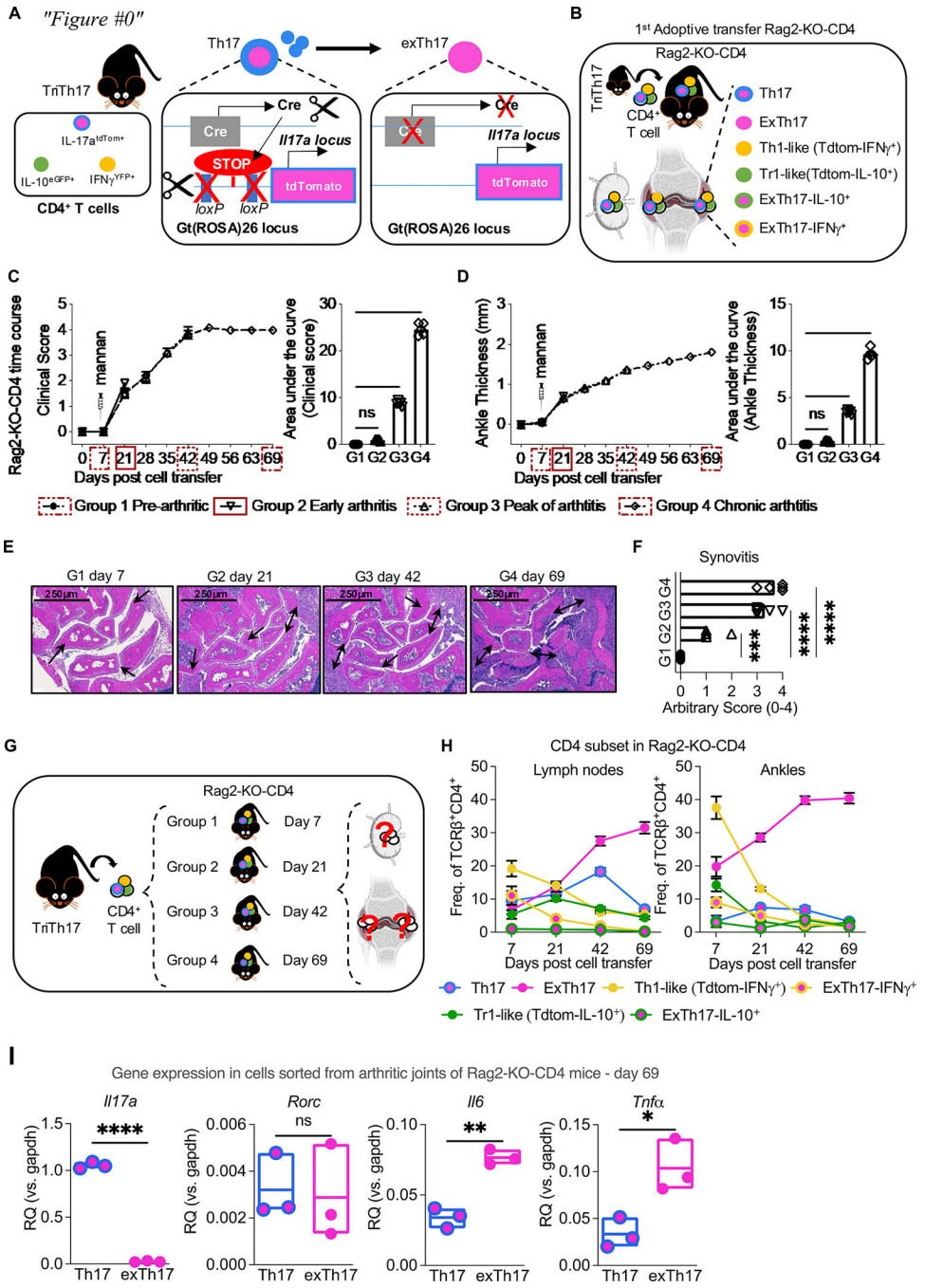

Figure 1. Th17 cells convert into exTh17 cells and become a prominent T cell population in joints and lymph nodes of SKG mice with chronic arthritis.

(**A**) Scheme of triple Th17 cell fate mapping SKG mice (triTh17 cell: B6.*Il17a*$^{Cre+/-}$.IL10$^{eGFP/eGFP}$.IFNg$^{YFP/YFP}$.R26tdTom$^{fl/fl}$.Zap70$^{SKG/SKG}$.H2$^{d/d}$) used as a source of cells for the experimental arthritis model.

(**B**) Scheme of arthritis model. TriTh17 CD4^{+} T cells (1×10^{6}) were adoptively transferred into Rag.B6.H2d (Rag2-KO) and arthritis severity and T cell fate in joint and lymph nodes were assessed.

(**C** and **D**) Time course of arthritis includes 4 time points (one group of mice per time point) with N=5 mice for each group. **C**) Arthritis assessment, evaluated by clinical score (left panel) with area under the curve (AUC, right panel). Boxes under the figure list time points utilized in Fig. 1E-H) Ankle thickness measurement (left panel) and AUC (right panel). Ankle thickness was plotted as the difference between measured thickness and baseline thickness for that timepoint. Statistics were calculated on the AUC.

(**E**) Representative histology for Rag2-KO-CD4 mice assessed at the indicated time points, H&E staining. Arrows indicate areas of inflammation.

(**F**) Histological quantification of synovitis at the indicated time points.

(**G**) End points for each group in time course of arthritis experiment (N=5 mice per point)

(**H**) Frequency (% of $TCR\beta^+CD4^+$) of T cell subpopulations (Th1, exTh1, Tr1-like ($Tdtom^-IL10^+$), Th1-like ($Tdtom^-$ $IFN\gamma^+$), ExTh17-$IL10^+$ and ExTh17-$IFN\gamma^+$ cells in lymph nodes (left panel) and joints (right panel) of Rag2-KO-CD4 from day 7 after $CD4^+$ T cell injection to day 69 of arthritis.

(**I**) mRNA expression of indicated genes in sorted Th17 cells vs exTh17 cells from arthritic ankles of Rag2-KO-CD4 (N=3). Graphs show relative quantification (RQ) versus housekeeping gene.

Graphs in (C, D and H) show grouped summary data plotted at mean ±SEM, each line corresponding to a different group of mice, and each point in histograms represents data from an individual mouse (statistics for H are shown in Fig. S2C). Histograms in (F, H, and I) show mean ±SEM and each point in histograms represents data from an individual mouse. (C, D and F) one-way ANOVA with Dunnett's multiple comparisons test, reference group is G1; (I) unpaired t-test; two-tailed. *p<0.05; **p<0.01; ****p<0.0001; ns: not significant.

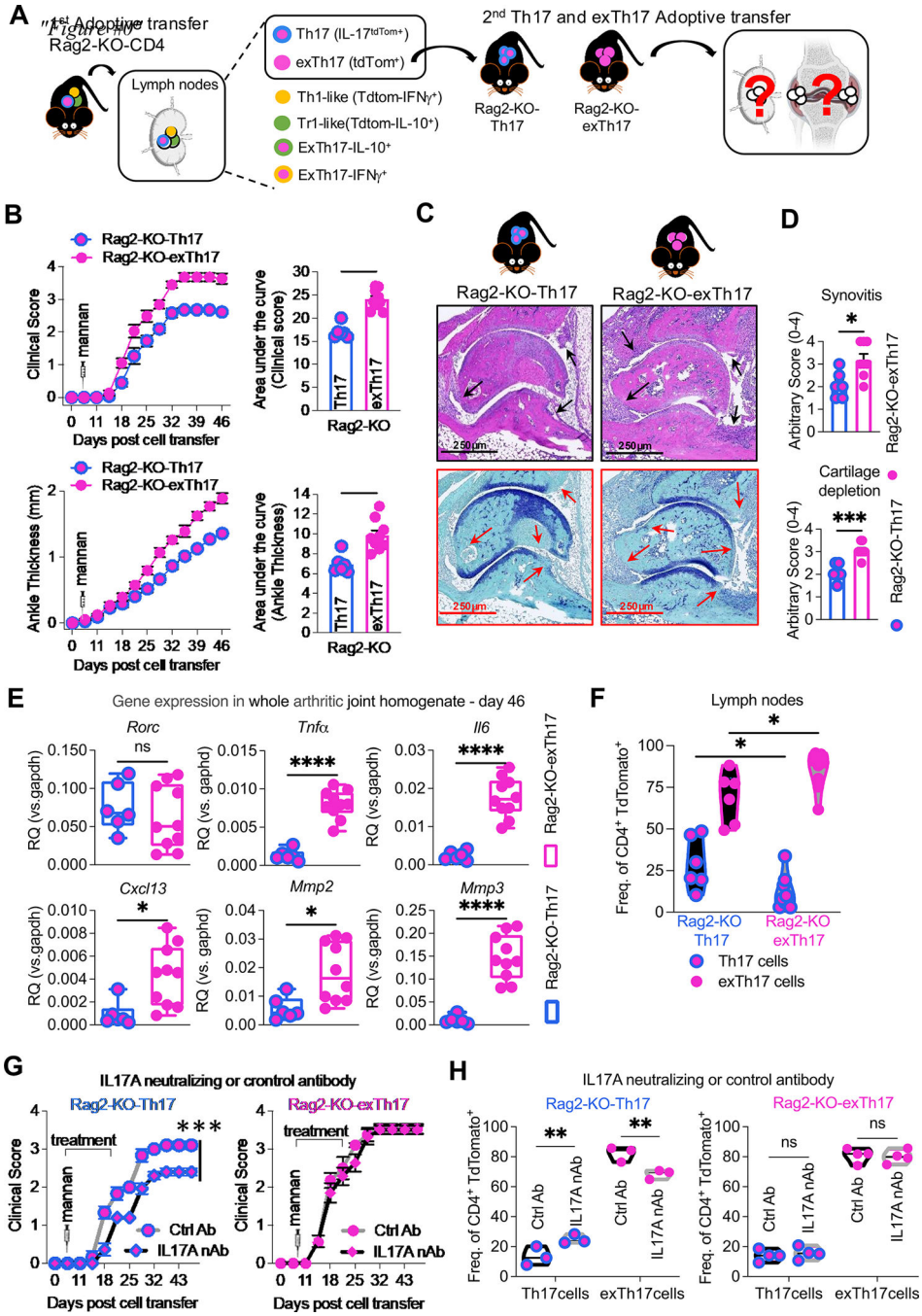

Figure 2. Higher arthritogenic potential of exTh17 cells vs Th17 cells in SKG arthritis does not depend on re-expression of IL-17.

(**A**) Scheme of arthritis model. Th17 cells vs exTh17 cells were sorted from lymph nodes of Rag2-KO-CD4 and 1×10^5 cells were adoptively transferred in Rag2-KO mice and arthritis severity and T cell fate in joint and lymph nodes were assessed.

(**B**) Arthritis assessment in female Rag2-KO-Th17 (N=6) and Rag2-KO-exTh17 (N=9) mice, evaluated by clinical score (upper panel) and ankle thickness measurement (lower

panel). Ankle thickness was plotted as the difference between measured thickness and baseline thickness for that timepoint. Statistics were calculated on the AUC.

(**C**) Representative joint histology from experiment in B.Rag2-KO-Th17 and Rag2-KO-exTh17 mice evaluated via H&E staining (black arrows indicating areas of synovitis, top panels) and toluidine blue staining (black arrows indicating areas of cartilage depletion, bottom panels) and (**D**) Histological quantification of synovitis (top graph) and cartilage depletion (bottom graph) from panel C.

(**E**) mRNA expression of indicated genes in joint homogenates from arthritic female Rag2-KO-Th17 and Rag2-KO-exTh17 mice from panel B. Graphs show relative quantification (RQ) versus *Gapdh* housekeeping gene.

(**F**) Frequency (% of $CD4^{+}TdTomato^{+}$) of Th17 and exTh17 cell populations in lymph nodes of arthritic female Rag2-KO-Th17 and -exTh17 mice from panel B.

(**G**) Arthritis assessment evaluated by clinical score of Rag2-KO-Th17 (left panel) and Rag2-KO-exTh17 (right panels) treated with IL-17A neutralizing (Clone 17F3) (Rag2-KO-Th17 N=3, Rag2-KO-exTh17 N=6) or isotype control Ab (Clone MOPC-21) (Rag2-KO-Th17 N=3, Rag2-KO-exTh17 N=4). Statistics were calculated on the AUC.

(**H**) Frequency (% of $CD4^{+}TdTomato^{+}$) of Th17 and exTh17 cells in lymph nodes of Rag2-KO-Th17 (left panel) and Rag2-KO-exTh17 (right panel) mice treated with IL-17A neutralizing (N=3) or isotype control Ab (N=3).

Graphs in (B and G) show grouped summary data plotted as Mean ±SEM, each line corresponds to a different group of mice and each point in histograms represents data from an individual mouse; graphs in (D, E, F and H) show mean ±SEM and each point represents data from an individual mouse.

(B, D and E) unpaired t-test; two-tailed (F and H) Two-way ANOVA with Šídák's multiple comparisons test; Interaction was significant for (F) (p=0.0013) and (H) Rag2-KO-Th17 (p= 0.0014) and not significant for (H) Rag2-KO-exTh17. *p<0.05; **p<0.01; ***p<0.001; ****p<0.0001; ns: not significant.

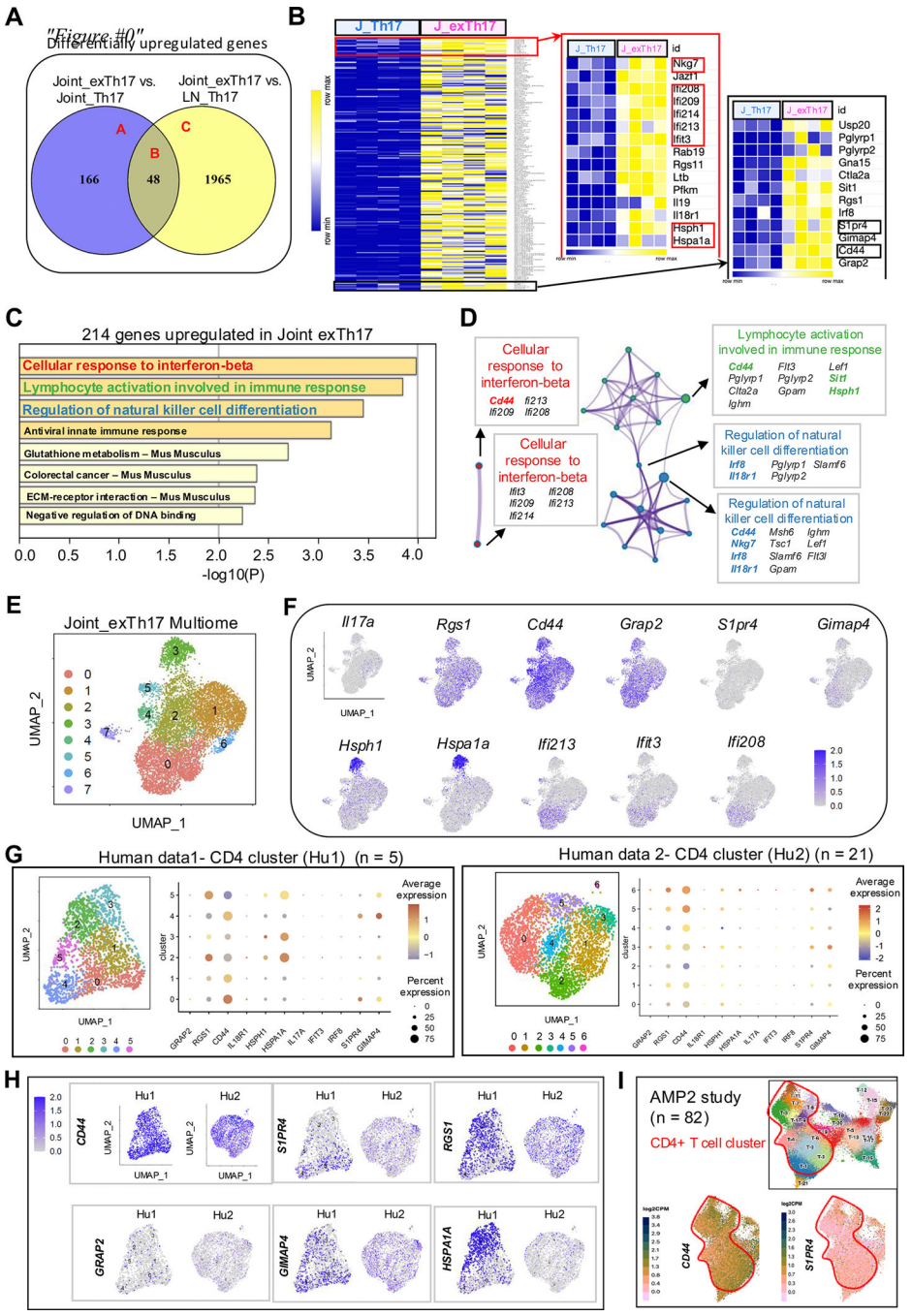

Figure 3. Integration of bulk transcriptome and single-cell multiome data highlight subclusters of exTh17 cells whose signature is found in RA synovium.

(**A**) Venn diagram showing different intersections of differential upregulated genes from bulk RNA-seq after pairwise analysis of joint Th17 cells (Joint_exTh17) vs joint exTh17 cells (Joint_exTh17) and Joint_exTh17 vs lymph node Th17 cells (LN_Th17). Intersection A and B in total include 214 genes upregulated in the Joint_exTh17samples. Each group (Joint_exTh17, Joint_Th17 and LN_Th17) represents a sorted population from female

arthritic Rag2-KO-CD4 mice with a N=4 replicates per group (each replicate representing a pool of 7–8 arthritic mice).

(**B**) Heatmaps of relevant genes from the 214 upregulated genes in Joint_exTh17.

(**C**) Pathway analysis on 214 upregulated genes in Joint_exTh17 vs Joint_Th17.

(**D**) Network layout from the entire set of 214 upregulated genes in Joint_exTh17 vs Joint_Th17 visualized using Cytoscape with “force-directed” layout and with edge bundled for clarity. Sub-pathways of each network are represented by circle nodes. The size of each circle is proportional to the number of genes within a pathway. Nodes with same color belong to the same main pathway from panel **C**. The network analysis shows the genes that are found highly expressed and involved in interactions between pathways.

(**E**) UMAP plot on data from 10x Multiome experiment performed on sorted exTh17 cells from arthritic joints of Rag2-KO-CD4 mice. Clusters were obtained using the weighted nearest neighbor (WNN) analysis in Seurat that utilizes both the RNA-seq and the ATAC-seq component for each cell. Clusters 8 and 9 with less than 100 cells were removed from downstream analysis.

(**F**) Feature plots showing single-cell level expression of selected genes among 214 that were identified as upregulated in Joint_exTh17 vs Joint_Th17 from bulk RNA-seq data.

(**G**) UMAP visualization, clustering and dot plots for selected genes of T cells from Wu et al. 2022 (PRJNA725073 – left panel – Human data 1 [Hu1]) (52) and human RA synovium $CD4^+$ T cells extracted from a single-center cohort (right panel – Human data 2 [Hu2], GEO Accession ID GSE303539). ~1800 and 3400 different CD4+ T cells were computationally extracted (more details in Fig. S5C), respectively from each study.

(**H**) Feature plots showing expression of selected genes using UMAP visualizations of scRNA-seq data for Hu1 and Hu2.

(**I**) Feature plots showing expression of exTh17 cell signature genes CD44 and S1PR4 using UMAP visualizations of scRNA-seq data for Accelerating Medicines Partnership (AMP) cohort(53).

"Figure 4"

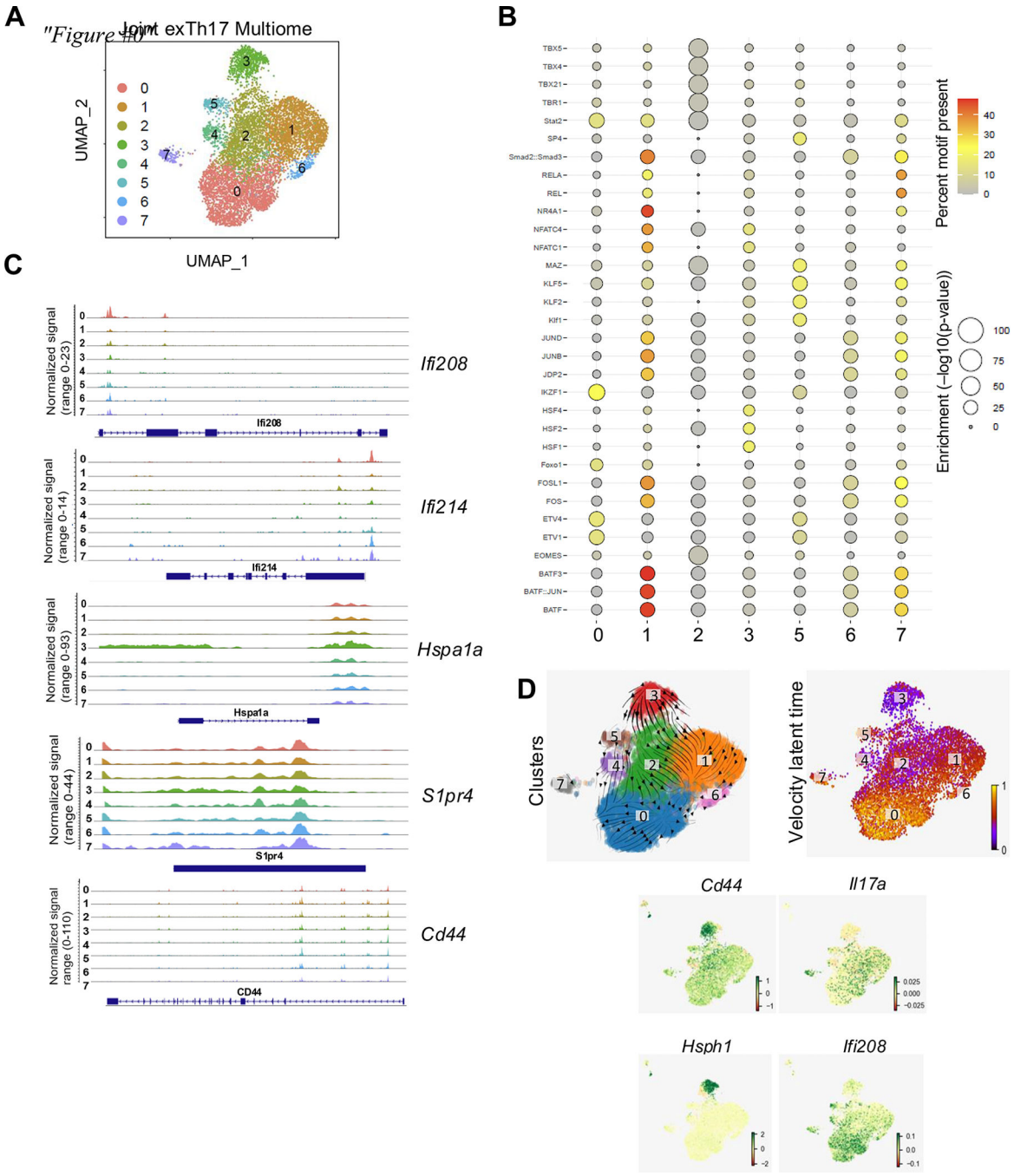

Figure 4. Single-cell chromatin accessibility and RNA velocity analyses highlight upstream cluster-specific regulators and potential checkpoints for exTh17 cell development.

(**A**) Top transcription factor motifs enriched in the marker ATAC-seq peaks upregulated in each cluster. Motif enrichments were obtained using *FindMotifs* function of Signac on the differentially accessible peaks across clusters. The top 4 TFs with most enriched motifs were extracted for each cluster and combined together for dot plot analysis. Color represents percent of marker ATAC-seq peaks with the occurrence of the specified motif. Cluster 4 did not have any TF with motif enrichment.

(**B**) Cluster-wise aggregated chromatin accessibility signal (ATAC-seq) for selected gene loci.
(**C**) Velocity vectors calculated using gene expression and ATAC-seq (multiVelo) visualized on the UMAP of Joint_exTh17 multiome data (top left panel) with pseudotime inferred from the velocity analysis visualized on the same UMAP (top right panel). Bottom panels show phase portraits derived from gene expression profiles of selected genes. A pool of 10 Rag2-KO-CD4 mice was used to sort exTh17 and Th17 cells from joints and lymph nodes.

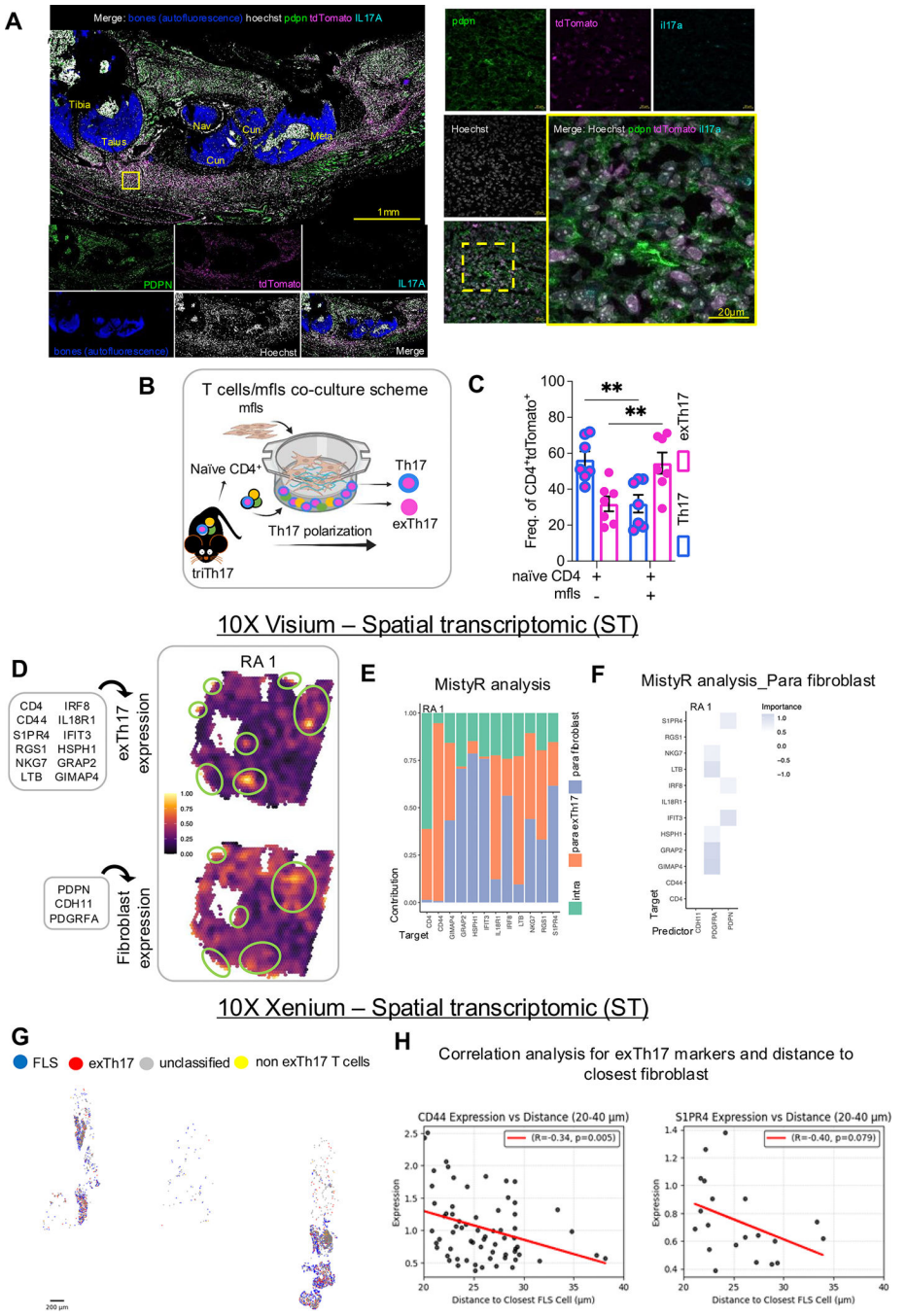

Figure 5. FLS can modulate the joint microenvironment to promote formation of exTh17 cells.

(**A**) Representative immunofluorescence images of calcified joint from arthritic Rag2-KO-CD4. Left panel shows an overview of the joint. Text boxes indicate relevant bones (Nav: navicular; Cun: cuneiform; Meta: metatarsal). High-resolution image of the area in yellow rectangle is shown on the right. IL-17A signal is turquoise, TdTomato is magenta, podoplanin is green, Hoechst is grey and bone autofluorescence is blue (only in left panel).

(**B**) Results from the co-culture assay using naïve $CD4^+$ T cells and mouse fibroblast-like synoviocytes (mfls) from 3 mice per replicate and 7 replicates for a total of 21 triTh17 mice. Graph shows frequency (% of $CD4^+$ $TdTomato^+$) of Th17 and exTh17 cells.
(**C**) Representative figure of co-expression analysis of N= 1 RA human synovium ST data. Boxes list genes used to define exTh17 cells (left) and FLS (right) in the deconvolution analysis. Green circles highlight co-localization spots.
(**D, E**) MistyR analysis of neighboring spots on samples RA 1. Bars indicate how much each view component (intra, para exTh17 cells and para fibroblast) contributes to explaining (predicting) the expression of exTh17 cell markers. Intra indicate exTh17 cell markers of the same spots, para exTh17 cells indicate exTh17 cell markers of nearby spots and para fibroblasts indicates FLS markers of nearby spots. (**E**) Plots quantifying each fibroblast component marker (x axes) in predicting the expression of exTh17 cell makers (y axes). A positive importance value indicates that the feature contributes to the prediction of a target.
(**F, G**) Spatial transcriptomic analysis (10X Xenium) on human synovium from RA patients F) Spatial plot of Xenium with cells colored by cell type. exTh17 cells are shown with red color and FLS cells are shown with blue color (Region 3). G) Negative correlation between exTh17 cell-to-FLS cell distance and expression of CD44 and S1PR4. Neighborhood analysis was performed to assess the relationship between gene expression in exTh17 cells and their spatial proximity to FLS cells in Region 3 and Region 4. Expression levels of CD44 and S1PR4 in exTh17 cells were negatively correlated with their distance to the nearest FLS cells, indicating higher expression in cells closer to FLS. Correlation coefficient for CD44: $R = -0.34$ (p-value = 0.05); for S1PR4: $R = -0.40$ ($p = 0.07$).
Graph in B shows mean ±SEM and each point represents data from a separate experiment. (B) Two-way interaction model between groups was significant ($p<0.0001$). Two-way ANOVA with Šídák's multiple comparisons test; 2-way factorial ANOVA Model was significant. **$p<0.01$.

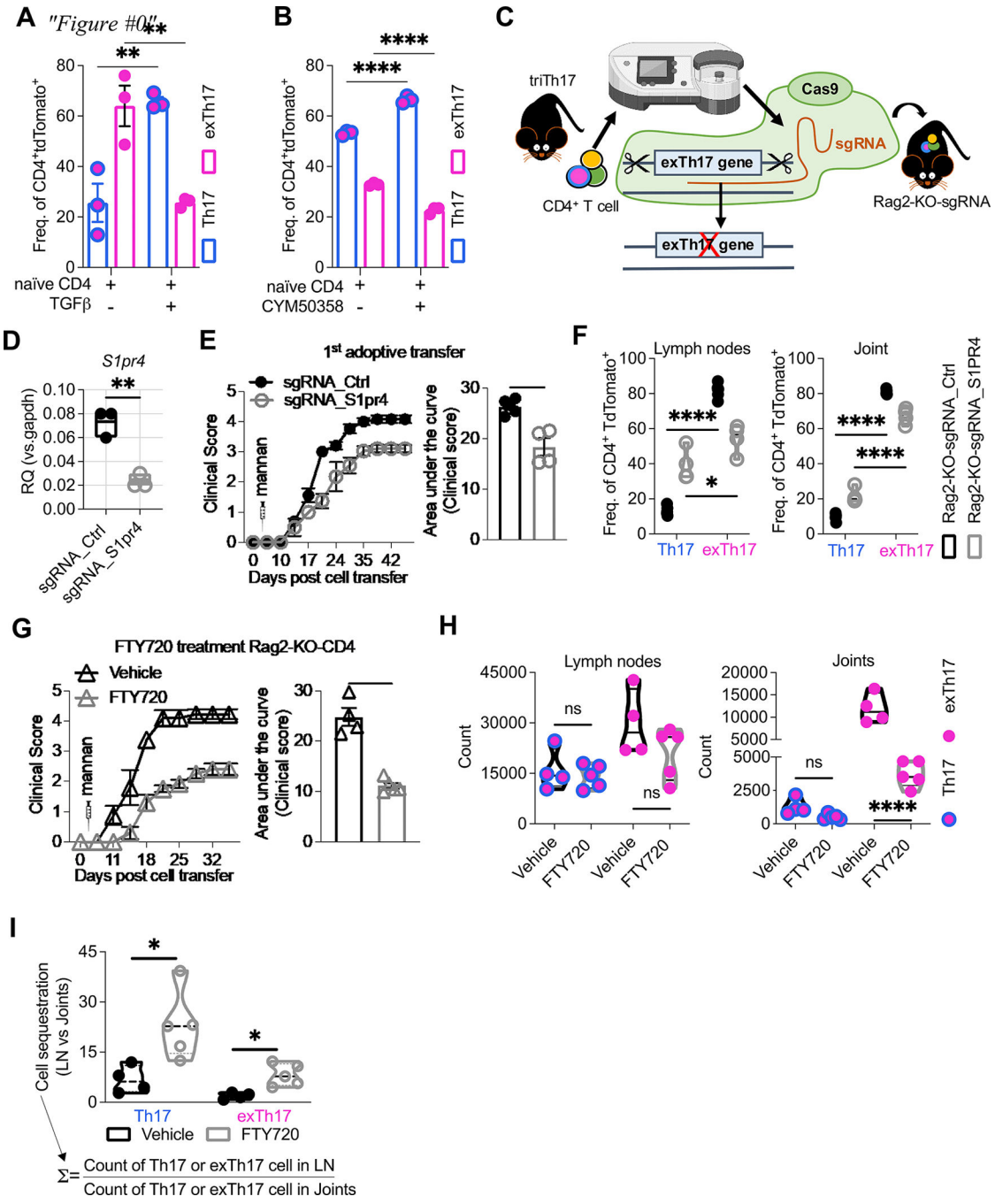

Figure 6. *S1pr4* contributes to joint exTh17 cell generation.

(**A**) Differentiation assay in the presence of mfls (as described in Fig. 5b) of naïve CD4$^+$ T from triTh17 mice, with (N=3) and without TGFβ (N=3). Graph shows frequency (% of CD4$^+$tdTomato$^+$) of Th17 and exTh17 cells in triplicate.(**B**) Naïve CD4$^+$ T cells from triTh17 mice were cultured in Th17cell polarization conditions for 5 days, with (N=3) and without S1PR4 antagonist (CYM50358) (N=3). Graph shows frequency (% of CD4$^+$tdTomato$^+$) of Th17 and exTh17 cells.

(**C**) Scheme of CRISPR/Cas9 mediated knock down of *S1pr4* in CD4+ T cells isolated from triTh17 mice before adoptive transfer into Rag2-KO mice.
(**D**) Expression level of *S1pr4* mRNA in $CD4^+$ T cells from triTh17 mice (N=4 mice, value represents a triplicate from cultured $CD4^+$ T cells) subjected CRISPR/Cas9-mediated knockdown prior to transfer into Rag2-KO mice in **E**. Graphs show relative quantification (RQ) versus housekeeping gene.
(**E**) Assessment of arthritis in Rag2-KO-CD4 mice after adoptive transfer with sgRNA_S1pr4 (N=4) or sgRNA_Ctrl (N=5) triTh17 $CD4^+$ T cells, evaluated by clinical score (left panel) with AUC (right panel). Statistics were calculated on the AUC.
(**F**) Frequency (% of $CD4^+tdTomato^+$) of Th17 and exTh17 cells in lymph nodes and joint of sgRNA_S1pr4 (N=4) or sgRNA_ctrl (N=5) Rag2-KO-CD4 mice.
(**G**) Assessment of arthritis in Rag2-KO-CD4 mice treated with either FTY720 (N=5) or vehicle (N=4) evaluated by clinical score (left panel) with AUC (right panel). Statistics were calculated on the AUC.
(**H**) Numbers of Th17 and exTh17 cells in lymph nodes (left graph) or joints (right graph) from Rag2-KO-CD4 mice treated with either FTY720 (N=5) or vehicle control (N=4).
(**I**) T cell sequestration in lymph nodes vs joints (Σ= counts of Th17 or exTh17 cells in lymph nodes / counts of Th17 or exTh17 cells in joints)
Histograms in (A and B) show Mean ±SEM and each point represents data from a separate experiment.
Graphs in (E and G) show grouped summary data plotted at Mean ±SEM, each line corresponding to a different group of mice, and each point in histograms represents data from an individual mouse. Graphs in (D, F, H, and I) show mean ±SEM and each point represents data from an individual mouse.
(A, B, F, H and I) 2-way ANOVA with Šídák's multiple comparisons test; Interaction was significant for (A) ($p=0.0001$), (B) ($p<0.0001$), (F) ($p<0.0001$), (H) joints ($p=0.0003$) and, (I) ($p=0.0001$) and not significant for (H) lymph nodes; (D, E and G) unpaired t-test, two-tailed; *$p<0.05$; **$p<0.01$; ****$p<0.0001$; ns: not significant.

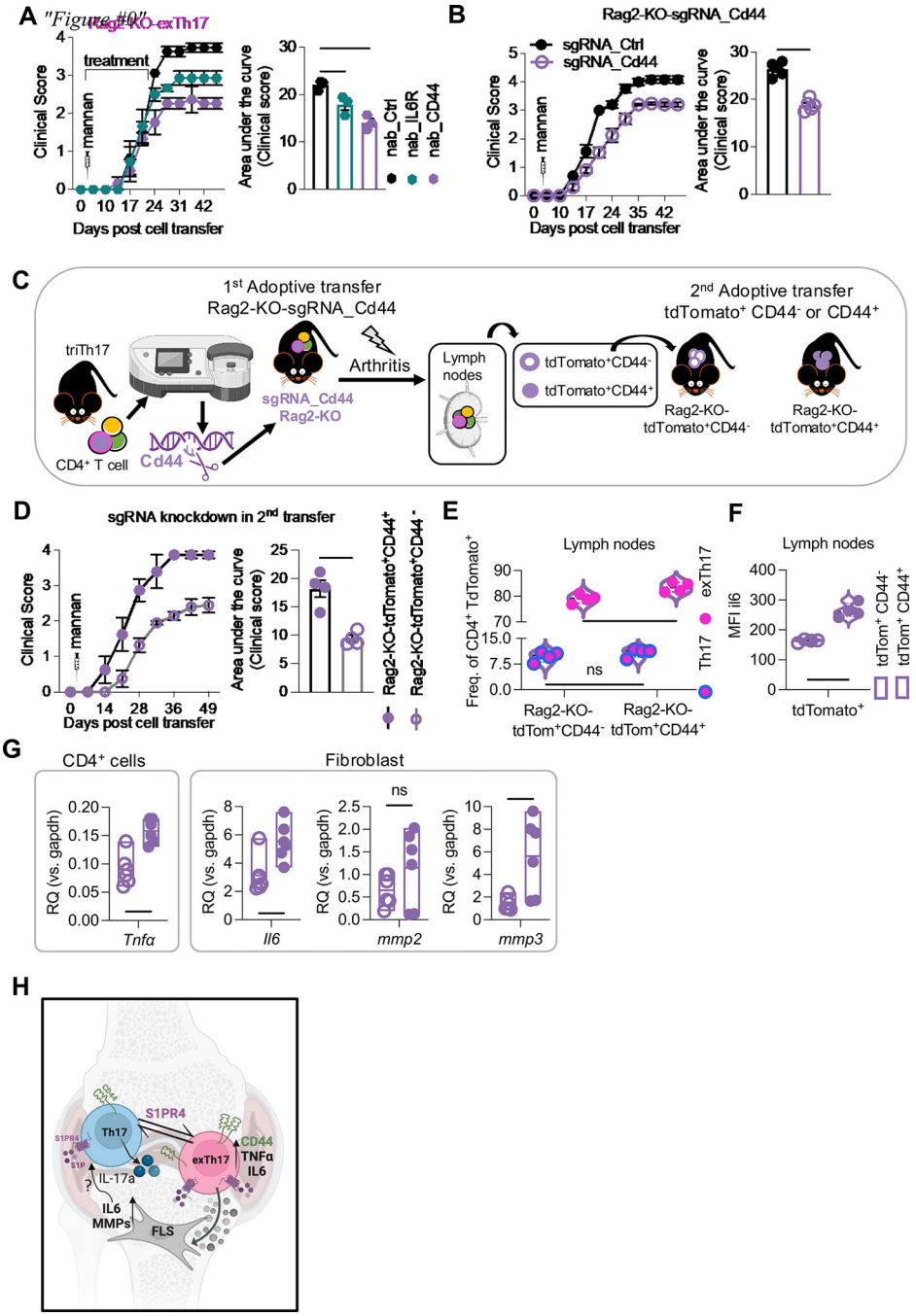

Figure 7. CD44 promotes the pathogenicity of exTh17 cells.

(**A**) Assessment of arthritis (left panel) and area under the curve (right panel) in Rag2-KO-exTh17 treated with either anti-CD44 (N=3), anti-IL6R (N=3) or isotype-Ctrl (N=3) Ab during the indicated time period.

(**B**) Assessment of arthritis (as performed in A) in Rag2-KO-CD4 mice after adoptive transfer with sgRNA_Cd44 (N=4) and sgRNA Ctrl triTh17 (N=4) $CD4^+$ T cells evaluated by clinical score (left panel) with AUC (right panel). Statistics were calculated on the AUC.

(**C**) Scheme of 2nd adoptive transfer of tdTomato$^+$CD44$^+$ and tdTomato$^+$CD44$^-$ cells isolated from arthritic Rag2-KO-sgRNA_Cd44 mice generated via adoptive transfer with sgRNA_Cd44 triTh17 CD4$^+$ T cells.
(**D**) Assessment of arthritis (performed as in **A**) in Rag2-KO mice after adoptive transfer with either tdtomato$^+$CD44$^+$ (Rag2-KO-tdTomato$^+$CD44$^+$) (N=4) or tdTomato$^+$CD44$^-$ (Rag2-tdTomato$^+$CD44$^-$) from Rag2-KO-CD4 (N=4) mice shown in **C**. Statistics were calculated on the AUC.
(**E**) Frequency (% of CD4+tdTomato+) of Th17 and exTh17 cells in lymph nodes from Rag2-KO-tdTomato$^+$CD44$^+$ (N=4) and Rag2-KO-tdTomato$^+$CD44$^-$ mice (N=4).
(**F**) Mean Fluorescence Intensity (MFI) of IL-6 in tdTomato$^+$ CD4$^+$ T cells from lymph nodes of Rag2-KO-tdTomato$^+$CD44$^+$ (N=4) and Rag2-KO-tdTomato$^+$CD44$^-$ mice (N=4).
(**G**) mRNA expression of key genes in CD4$^+$ T cells or FLS sorted from the joints of arthritic Rag2-KO-tdTomato$^+$CD44$^+$ (N=2) and Rag2-KO-tdTomato$^+$CD44$^-$ mice (N=2), in technical triplicate.
(**H**) Working model for interplay between Th17-exTh17 cells conversion and FLS pathogenicity in SKG arthritis synovium.
Graphs in (A, B, and D) show grouped summary data plotted at Mean ±SEM, each line corresponding to a different group of mice, and each point in histograms represents data from an individual mouse. Graphs in (E and F) show Mean ±SEM and each point represents data from an individual mouse. Graphs in (G) show Mean ±SEM and each point represents a technical replicate.
(A) Dunnett's multiple comparisons test, reference group is the control antibody group; (E) one-way ANOVA with Šídák's multiple comparisons test; Interaction was not significant. (B,D, F and G) unpaired T test, two-tailed; *p<0.05; **p<0.01; ***p<0.001; ****p<0.0001; ns: not significant.